An Experimental Investigation of Pressure Distributions on a Straked Cylinder

by

Maneesh Kumar

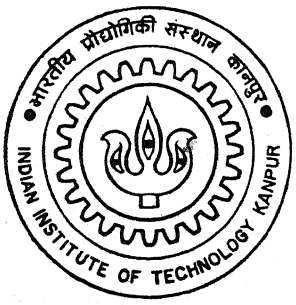

DEPARTMENT OF AEROSPACE ENGINEERING

INDIAN INSTITUTE OF TECHNOLOGY KANPUR

APRIL, 1996

An Experimental Investigation of Pressure Distributions on a Straked Cylinder

A Thesis Submitted

in Partial Fulfillment of the Requirements

for the Degree of

Master of Technology

by

Maneesh Kumar

to the

DEPARTMENT OF AEROSPACE ENGINEERING

INDIAN INSTITUTE OF TECHNOLOGY, KANPUR

April, 1996

AE-1996-M-KUM-EXP

CERTIFICATE

It is certified that the work contained in the thesis entitled "*An Experimental Investigation of Pressure Distributions on a Straked Cylinder*", by Mr. *Maneesh Kumar*, has been carried out under my supervision and that this work has not been submitted elsewhere for a degree.

A. K. Gupta

(Dr. A. K. Gupta)

Professor

Department of Aerospace Engineering,

Indian Institute of Technology,

Kanpur.

April,1996

To

Mummy and Daddy

ABSTRACT

The cylindrical structures are prone to suffer damage due to the oscillations caused by the periodic shedding of vortices from the structure. Several devices for reduction of vortex-induced oscillations have been used in past. In the present investigation, the effect of helical strake on the pressure distribution of a circular cylinder has been investigated. For this a cylindrical model with helical strake was tested in a low speed wind tunnel. The pressure distributions show strong asymmetry both along the span as well as upwards and downwards/forward and backward regions at each span. This strong asymmetry is caused by the three dimensionality of the mean flow, introduced by the helical strake. Also, this three dimensionality of mean flow is likely to be responsible for the breaking up of fluctuating flow field which in turn is responsible for reduction in vortex-induced oscillations of cylindrical structures.

ACKNOWLEDGEMENTS

I take this opportunity to express my deep sense of gratitude to Dr. A.K. Gupta for the constant inspiration, support and encouragement given to me, not only during the course of this thesis, but at other critical times of my M.Tech. programme. His exemplary guidance and commendable patience benefitted me immensely in completing this work.

I would like to thank Mr. Bhattacharya and Mr. Mohan, Technical officer of Aerospace Workshop and Low Speed Aerodynamics Lab respectively for the help they provided in making the model and conducting the experiments. Help of Mr. Rameshwar, helper Aerodynamics Lab, in making the model is also appreciated.

Finally, I would like to extend my gratitude to my family and my friends for providing suggestions and encouragement at every stage through out the work.

NOMENCLATURE

α_{hs}	Angle Showing Strake Position w.r.t Flow Direction
α_{sp}	Angle Showing the Location of Radial Station, at which the Spanwise Distribution of Pressure is Measured, w.r.t Flow Direction
C_p	Coeffecient of Pressure
C_{ps}	Coeffecient of Pressure for Spanwise Distribution
D	Cylinder Diameter
P	Pressure at the Surface of the Cylinder.
P_∞	Free Stream Static Pressure.
ρ	Density of Air.
U_∞	Free Stream Flow Velocity.

Contents

List of Tables

List of Figures

Chapter 1

INTRODUCTION

1.1 Introduction

Whenever a vortex is shed from a bluff body, it alters the local pressure distribution, and the body experiences a time varying force at the frequency of vortex shedding. Many structures of engineering importance are usually slender with a bluff body cross-section and are prone to suffer this kind of adverse effect. Under certain conditions, sustained oscillations can be excited over a flow speed range and the structure oscillates at a frequency close to its natural frequency.

The mechanism of vortex shedding behind a circular cylinder and the oscillations related to it have been studied for more than a century but our understanding is still incomplete [1-4]. The suppression of these vortex-induced oscillations of circular cylinders has been the subject of considerable experimental investigations. A wide variety of aerodynamic and hydrodynamic means for suppressing these oscillations have been suggested [5].

These have been put in three categories which are as follows:

1. Surface protrusions(strakes, wires, fins, studs, or spheres, etc.)

2. Shrouds(perforated, gauze, axial rods and axial slats, etc.)

3. Nearwake stabilizers(splitter and s-tooth plates, guiding plates and vanes, base-bleed, slits cut along the cylinder, etc.)

Wong and Kokkalis[12] did a study of three aerodynamic devices, viz. Perforated shroud, Helical strake and Slat device and showed that all the three devices are effective in suppressing vortex-induced oscillations.

The helical-strake device as a vortex shedding eliminator was originally proposed by Scruton and Walshe [6]. Here a three dimensional flow is introduced which interferes with the periodicity of the shedding of two-dimensional vortices. In the past, several experimental investigations have resulted in the development of helical strake dimensions effective enough to be employed mainly on steel chimneys. The present experimental investigation attempts to investigate the effect of helical strake on the details of flow past a circular cylinder.

1.2 Literature Review

Scruton and Walshe [6] developed efficient surface protrusions for avoiding wind-exited oscillations of cylindrical structures. Three strakes of sharp-edged rectangular section were wound as three helices around the surface of the cylinder, with a pitch

of 15D. It was found that the attachment of quite a low height strake, h=0.029D, was effective in reducing the aerodynamic excitation. Some small improvement was effected by making h=0.059D, with a notable shift of critical velocities. Further increase to 0.088D was accompanied by a further increase of critical reduced velocity at which maximum amplitude occurred.

Woodgate and Maybrey [7] carried out tests to determine the optimum pitch for the three strakes. The outcome was a reduction of pitch from the original 15D to 5D, whilst the height of the strakes remained at 0.09D (except for light or lowly damped structures for which they advised an increase in height to 0.12D). The effectiveness of the system was not impaired by a gap of 0.005D between the strake and the cylinder surface. It has been proved sufficient to apply strakes only to the top third of a chimney stack to prevent instability in the fundamental mode (the general principle is to apply strakes in the region of antinodes).

Cowdrey and Lawes [8] measured the drag coefficient of a cylinder fitted with helical strakes. The drag coefficient was found to be almost constant from the high subcritical regime ($\mathrm{Re} = 1 \times 10^5$) , through the critical regime upto the postcritical one ($\mathrm{Re} = 4 \times 10^6$). This implies that the same flow pattern persists throughout that Reynolds number range. The values of the drag coefficients measured for two heights of strakes, 0.06D and 0.12D, were found to be 1.35 and 1.45, respectively. These values are high, particularly in the critical regime where the clean cylinder had a drag coefficient of less than 0.5.

Some further tests on the helical strakes were carried out by Ruscheweyh [9],

confirming that the optimal pitch is between 4D and 5D and that only top 1/3 of the cylinder height should be covered for the Reynolds number range from 1.8×10^4 to 4.0×10^4.

Vickery and Watkins [10] carried out tests in water and found that helical strakes were as effective as they were in air in suppressing oscillations of a single cylinder. The wind tunnel tests on a group of four plain and straked cylinders revealed that the addition of strakes was less effective in reducing the amplitudes of vibration of downstream cylinders.

Finally, Gartshore et al. [11] noticed an unexpected effect of free stream turbulence on the effectiveness of the three helical strakes. The tests were carried out in a wind tunnel on a two-dimensional elastically supported model and results presented in terms of the ratio of the maximum r.m.s. deflection of a model fitted with strakes to the maximum r.m.s. amplitude of the clean cylinder. When the model was submerged in a smooth flow the helical strakes reduced the amplitude of vibration at the critical velocity by a factor of ~ 100. The maximum response, at the elevated reduced velocity of 8, decreased in amplitude by a factor of 18.

Unexpectedly, the effectiveness of helical strakes diminished when the cylinder was submerged in a turbulent flow (14% intensity). The maximum amplitude of vibration of a clean cylinder was about half that found in smooth flow, but the helical strakes reduced this amplitude by only a factor of 5. At the elevated reduced velocity of 8, the reduction factor was only 2. The important conclusion drawn was that the effectiveness of strakes decreases with the intensity of turbulence of the free

stream and with increasing reduced velocity for a model having the same damping.

1.3 Present Work

All the experiments conducted on cylinders with helical strakes show that by using helical strakes the vortex-induced oscillations are reduced. In the present work, experiments were conducted to find out the change in pressure distribution around the cylinder by using helical strake on the surface of cylinder. So the aim of the present work was to find out the angular and spanwise pressure distribution on the surface of straked cylinder. The pressure distribution has to be compared with the respective pressure distributions on the clean cylinder.

The tests were conducted in a low speed wind tunnel on a cylinder of diameter 3.5 inches. The length of the cylinder was 24.0 inches (i.e. 2.0 fts.). The single start pattern of helical strake was used with the strake height of 0.47 inch and strake width of 0.16 inch. The strake pitch was 12.25 inches. The tests were conducted at the flow speeds of 4.5 m/s and 9.0 m/s. The tests were conducted for twelve flow configurations depending upon the location of strake at the centre of cylinder.

Chapter 2

EXPERIMENTAL SET-UP AND PROCEDURE

2.1 Wind Tunnel

The experiments for the present work were conducted in a low turbulence low speed wind tunnel. It is an open circuit low speed wind tunnel with a test section of 2'X2'X10'. It has a contraction ratio of 16 and turbulence level of 0.2%. It can give a maximum wind speed of 130ft./sec. The diffuser half angle is about 5^{o}.

Figure 2.1 shows the schematic diagram of the wind tunnel.

A 25 H.P. DC motor drives a blade propeller fan of 5' diameter. The motor is connected to a supply of 230 Volts AC through a voltage variac by which the voltage can be varied from 0 to 230 Volts and also through a voltage stabilizer ensuring constant speed.

The velocity of air through the test-section is controlled by varying the voltage

variac. A hole is made in the side wall of test-section for putting the pitot-static tube to measure the test section free stream speed.

2.2 Other Equipments

Other major equipments used to perform the experiments were:

1. Pitot-static tube for measuring the wind speed inside the test-section. The tube was put through the side wall and its head was located at a location which was 6.0 inches from the side wall. The two ports of the tube were connected to an electronic digital micromanometer which gave the free stream wind speed inside the test section directly in m/s.

   Figure 2.2 shows the schematic diagram of the pitot-static tube.

2. Electronic digital micromanometers for reading the values of pressure and wind speed. This manometer can give both the wind speed or the ΔP. Two manometers were used, one for measuring ΔP and one for wind speed. The manometer has two ports. At the positive port the tube from the pressure port was connected and at the negative port the tube from the static port of the pitot-static tube was connected.

   Figure 2.3 shows the photograph of the micromanometer with the multiport device.

3. Thermometer for measuring the ambient temperature.

2.3 Model

A hollow PVC cylinder of external diameter 3.5 inches was used to make the model. Hard rubber material was used for the strake, which had a rectangular cross-section. To make the model, the rubber material was attached helically around the basic cylinder according to the following particulars:

Single start pattern

Strake pitch	3.5D
Height of strake	0.134D
Width of strake	0.0446D

For attaching the helical strake, first of all a groove of the same pitch was cut on the surface of the cylinder. This groove was cut on a Milling Machine in the workshop of the Department of Aerospace Engineering at I.I.T. Kanpur. This groove was made to provide a firm support to the strake at the surface of the cylinder. Also this was meant for preventing the strake from flying off while running the tunnel. Then the rubber material was cut with the help of a sharp knife. Actually it was very difficult to cut the rubber material uniformly because of its elastic nature. So, it was cut very patiently and very cautiously, in a rectangular cross section, with the help of a sharp knife. It took several attempts before the material could be cut successfully. After cutting the material another difficulty arose in pasting it properly and uniformly. To solve this problem, instant fixing adhesive was used.

The cylinder was pressure tapped at the mid-span at twelve stations on the surface, separated from each other by an angle of 30^{o}. Also the cylinder was pressure

tapped in the spanwise direction at 18 stations, separated from each other by a distance of 1.25 inches, starting from the central position. Steel tubes of 1.5 mm diameter were used for pressure tappings. These steel tubes were then connected to the rubber tubes and were taken out of the model. For pasting these steel tubes tightly (to avoid any leakage), the same instant fixing adhesive was used. This adhesive blocked some of the steel tubes which were cleaned by manually drilling them with a drill of smaller size.

Figure 2.4 shows the photograph of the model with wooden fixture and pressure tubes.

Before attaching the helical strake the experiments for clean cylinder were conducted.

2.4 Experimental Set-up

The experiments for the present work were performed in the "Low Speed Aerodynamics Lab" of the Department of Aerospace Engineering at I.I.T. Kanpur. An open circuit wind tunnel with a closed rectangular test-section 2 ft. high, 2 ft. wide and 10 ft. long was used.

The straked cylinder was mounted vertically with the help of a wooden fixture. Radial lines, separated by 30^o were made on the fixture so that cylinder can be rotated easily in steps of 30^o. The tubes from all the 30 pressure ports were taken

out through wooden fixture and they were numbered 1 to 30. These tubes were connected to a multiport device from which one can select one port at a time. Through this device the counter was connected to an electronic digital micromanometer which gives the pressure reading in millimeters of water.

The pitot-static tube was inserted inside the test-section through a small hole in the side wall of the test-section. It was inserted near the model, upstream of it. The tubes from the two ports of pitot-static tube were connected to another electronic digital micromanometer, which served as an anemometer and gives directly the wind speed in m/s. Also from the static port of pitot-static tube another tube was connected to the reference port of the micromanometer, which was being used for measuring pressure. So, now this micromanometer directly gives the value of ΔP.

Figure 2.5 shows the photograph of test-section with complete experimental setup for the straked cylinder.

Similar set-up was made for the clean (without strakes) cylinder.

2.5 Experimental Procedure

The present work aims at measuring the pressure distribution around and along the cylinder, with the helical strake, on its surface. Then these pressure distributions are compared with the pressure distribution on the clean cylinder.

The experiments were performed in an open circuit subsonic wind-tunnel with

a closed rectangular test-section. The procedure adopted in conducting the experiment is described below.

First of all, the model was mounted and necessary connections were made as described in section 2.3. Then the ambient temperature was noted down with help of a dial thermometer fitted to the wind-tunnel.

The tunnel was then turned on. By controlling the voltage of its blower the tunnel speed was increased to the required velocity as indicated by the anemometer. The experiments were performed for two velocities of 4.5 m/s and 9.0 m/s. Now the counter connected to the micromanometer was set corresponding to the station number 1. The reading shown by micromanometer, digitally, in terms of millimeters of water corresponds to the pressure at the station number 1. The counter was then shifted from 1 to 30, and pressures at the corresponding stations noted down.

After noting down one complete set of 30 readings, the cylinder was rotated by 30^o to bring in different strake configuration relative to the wind direction. Once again 30 readings were taken. In the similar fashion, the cylinder was rotated by 30^o after each set of reading and in this way the twelve sets of readings were taken. Afterwards the speed was changed to a higher value and again twelve sets of readings were taken.

2.6 Analysis

After noting down all the readings of ΔP, the value of C_p (coefficient of pressure) was calculated. This value was plotted against angle for the pressure distribution around the circular cylinder and against the spanwise position for the spanwise pressure distribution. On the same plots the pressure distribution for clean cylinder was also plotted.

The expression used for calculating the value C_p is as follows:

$$C_p = \frac{P - P_\infty}{\frac{1}{2}\rho {U_\infty}^2} \tag{2.1}$$

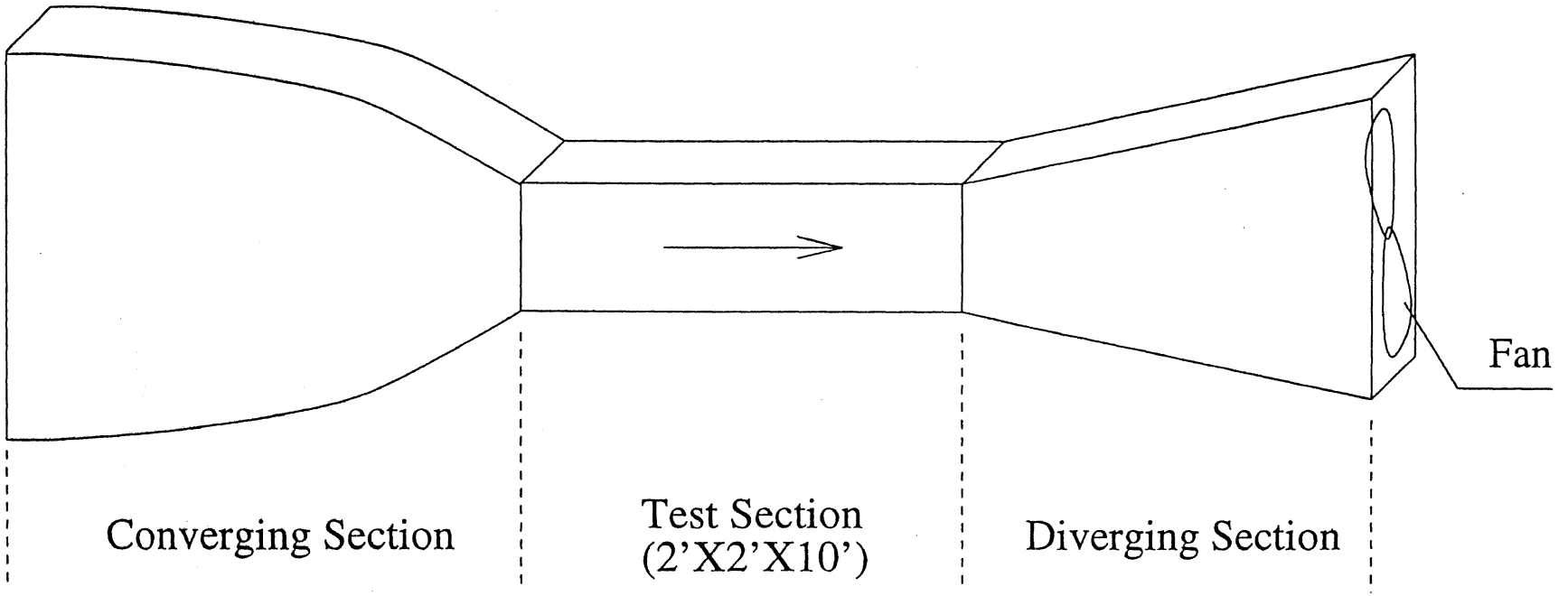

Figure 2.1: Schematic Diagram of Wind Tunnel (not to scale)

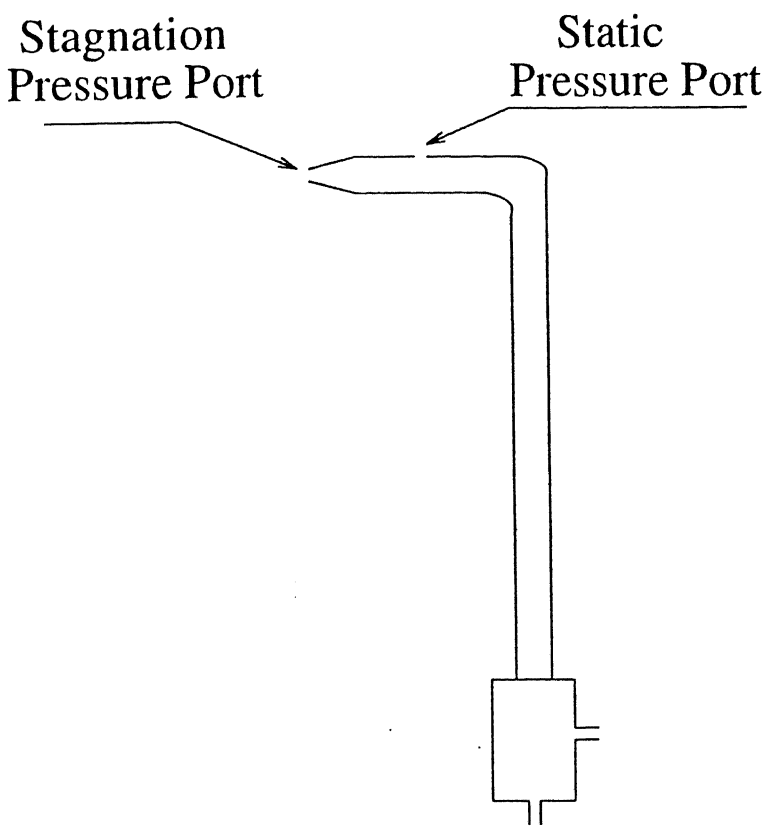

Figure 2.2: Schematic Diagram of Pitot-static tube(not to scale)

Figure 2.3: Electronic Digital Micromanometer with Multiport Device

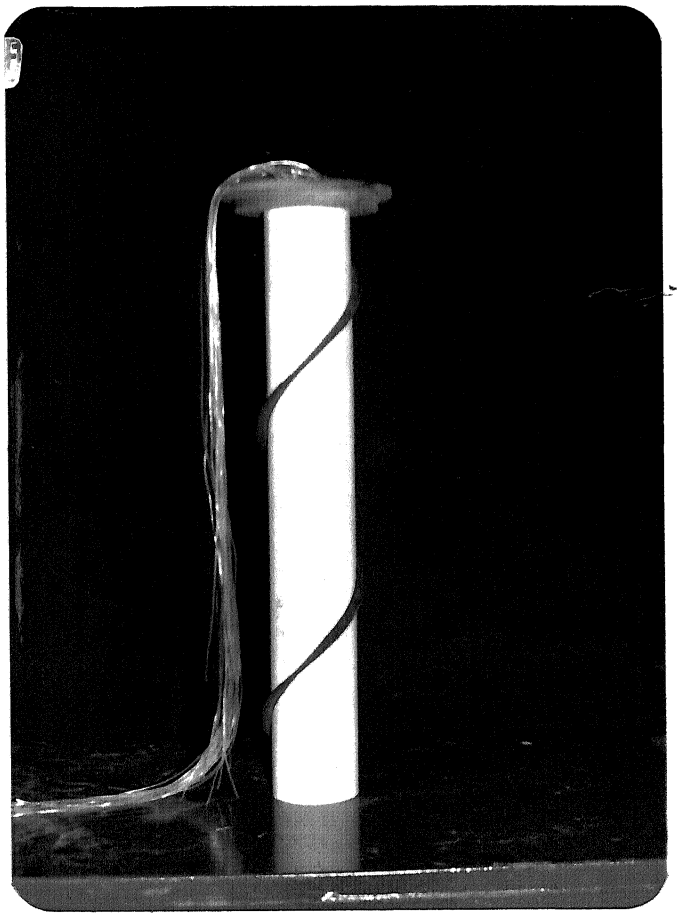

Figure 2.4: Model with Wooden Fixture and Pressure Tubes

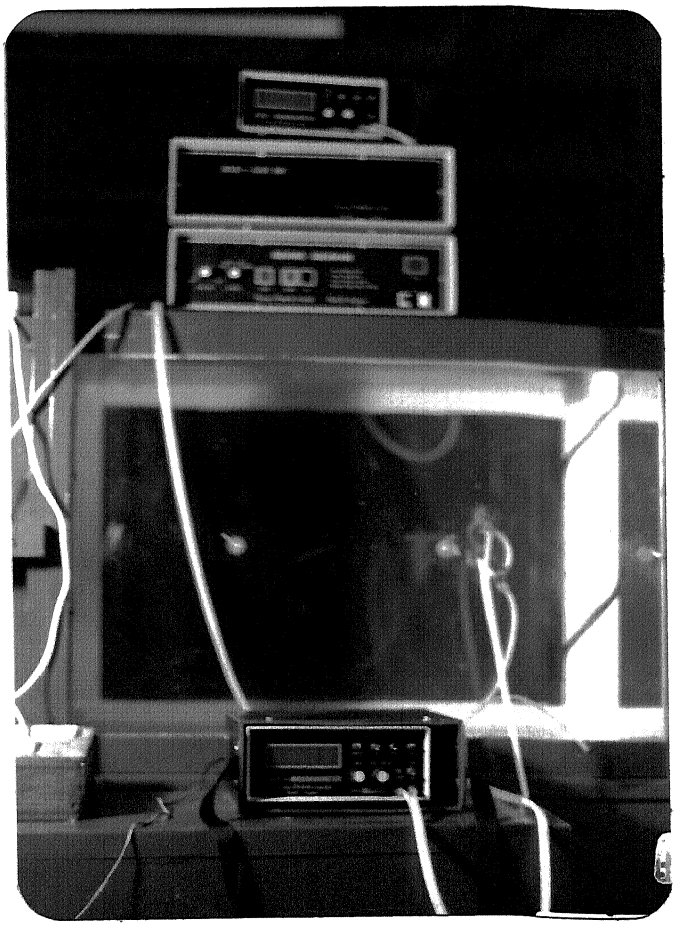

Figure 2.5: Wind Tunnel Test-section with Complete Experimental Setup

Chapter 3

RESULTS AND DISCUSSIONS

The aim of the present work was to investigate the pressure distributions on the surface of a circular cylinder with helical strake. The pressure distributions around the cylinder and along the cylinder were measured. these pressure distributions when compared with the pressure distributions of clean cylinder, show the effect of helical strake on the pressure distributions of a circular cylinder.

The helical strake introduces a three dimensionality in the mean flow field of the circular cylinder. The vortex shedding and associated oscillations are related to the fluctuating flow field, investigation of which is beyond the scope of this thesis. For investigating fluctuating flow field, a separate study needs to be done. One can only predict the variations in fluctuating flow field on the basis of the variations in mean flow field.

The experiments were conducted at two flow velocities of 4.5 m/s and 9.0 m/s, and for twelve flow configurations based on the location of strake at the centre of

the cylinder w.r.t. the flow direction (refer Fig. 3.1).

3.1 Pressure Distributions Around the Cylinder

Pressure distributions around the cylinder have been investigated at the mid-span of the circular cylinder. Pressures are presented non-dimensionally in the form of coefficient of pressure (C_p), defined earlier. The reference velocity and static pressure are taken as those just upstream of the cylinder.

The values of C_p are plotted radially on a circular cylinder as shown in figs. - to - . In these plots the value of C_p is zero on the surface of the cylinder. The positive and negative values are plotted inside and outside the cylinder respectively.

The pressure distributions show a similar trend at the two speeds. Here the pressure distribution curves for $U_\infty = 4.5$ m/s are discussed in detail. This analysis also applies to the curves at the wind speed of 9.0 m/s with a slight change in exact values which are tabulated in appendix A.

The effect of the helical strake on the pressure distributions can be studied by dividing the location of strake at the centre of the cylinder in three regions which are as follows:

1. Forward Region (For $\alpha_{hs} = 0^o$ to $\pm 20^o$)

2. Midriff Region (For $\alpha_{hs} = \pm 20^o$ to $\pm 85^o$)

3. Rear Region (For $\alpha_{hs} = \pm 85^o$ to $\pm 180^o$)

For definition of α_{hs}, refer Fig. 3.1.

Forward Region

The radial pressure distribution at the centre of the cylinder shows no local peaks at or near the location of the strake. However the presence of strake in the forward region does modify the pressure distribution such that in the midriff and rear region of the cylinder the pressures are slightly higher than the pressure values for a clean cylinder. The pressure distributions in the forward region of the cylinder is almost the same as that for a clean cylinder. So the only effect is a slightly higher pressure in the midriff and rear regions of the cylinder. The pressure distribution curves for this region of strake location are shown in Fig. 3.3, 3.4, 3.15 and 3.16.

In the forward region of strake location Fig. 3.3 and Fig. 3.4 are very much alike.

Midriff Region

When the strake is in this region then the pressure peaks are observed near the location of strake and also, at other points, a slightly higher pressure is observed. The pressure distribution in the forward region of cylinder remains unchanged. These peaks bring strong asymmetry in the local mean flow field as the upper and lower surfaces show two different pressure distribution unlike the clean cylinder. The pressure distribution curves for midriff region of strake location are shown in Fig. 3.5 to Fig. 3.8 and Fig. 3.17 to Fig. 3.20.

In this region of strake location Fig. 3.5 and Fig. 3.7 are very much similar. In both the cases the pressure becomes very less just downstream of the strake location.

This happens because of the excessive separation of the flow over the strake. Also upstream of the strake, the region of positive pressure increases because of the blockage of flow by the strake.

In Fig. 3.5, the value of C_p just downstream of strake location becomes -2.60 as compared to -1.14 for a clean cylinder. Similarly in Fig. 3.7, the value of C_p just downstream of strake location was -1.92 as compared to -1.51 for the clean cylinder.

Also, Fig. 3.6 and Fig. 3.8 are very much similar. Here also, in both the cases the pressure becomes very less just downstream of the strake location because of the excessive separation of flow over the strake. The pressure upstream of the flow is quite high because of the blockage of flow by the strake.

In Fig. 3.6, the value of C_p just downstream of strake location becomes -1.86 as compared to -1.42 for a clean cylinder. Similarly in Fig. 3.8, the value of C_p just downstream of strake location was -2.04 as compared to -1.40 for the clean cylinder.

One can easily see a more disturbed and asymmetric local flow field in the midriff region of strake location compared to forward region of strake location. This disturbance in the local flow field in the midriff region is caused because of the excessive separation of the flow over strake.

Rear Region

In this region the effect of strake is similar as in the case of forward region i.e. No local pressure peaks are observed near the location of strake. However slightly higher pressures are observed in the midriff and rear regions of the cylinder as compared with the pressure values for a clean cylinder. The pressure distributions in the

forward region of cylinder are almost the same as that for a clean cylinder. The pressure distribution curves for this region of strake location are shown in Fig. 3.9 to Fig. 3.14 and Fig. 3.21 to Fig. 3.26.

All the figures in this region are very much alike. Also, these figures are similar to the Figures 3.3 and 3.4 of the forward region. So, one can say that the effect of strake location in forward and rear region is same.

The local flow field more disturbed and asymmetric in case of the strake location in the midriff region as compared to the rear region of strake location because flow in rear region is already separated and further separation by strake is not possible.

3.2 Pressure Distributions Along the Cylinder Span

Spanwise pressure distributions are plotted on a rectangular plot alongwith the pressure distributions for a clean cylinder. The spanwise pressure taps were made only at one radial position. Everytime by rotating the model by 30°, the spanwise pressure distributions at all the twelve positions were measured. The flow configuration for all the twelve positions were different because of the three dimensionality introduced by the helical strake.

The pressure distributions show a similar trend at the two speeds. Here the pressure distribution curves for $U_\infty = 4.5$ m/s are discussed in detail. This analysis also applies to the curves at the wind speed of 9.0 m/s with a slight change in exact

values which are tabulated in appendix A.

On a clean cylinder, pressure doesn't vary in spanwise direction. But on a straked cylinder the flow doesn't remain two dimensional, so the pressure also varies in spanwise direction. In some of the flow configurations, there is not much of pressure variation in spanwise direction. In others there are pressure peaks depending upon the strake position vis-a-vis the pressure taps.

Here one can divide the spanwise pressure curves depending upon the location of the point at the mid-span of the cylinder where spanwise distribution has been measured, w.r.t. the flow direction. This is characterized by an angle α_{sp} as shown in Fig. 3.2. Once again the whole range can be divided in three regions, for considering the spanwise pressure distributions, based on α_{sp}.

1. Forward Region (For $\alpha_{sp} = 0^o$ to $\pm 25^o$)

2. Midriff Region (For $\alpha_{sp} = \pm 25^o$ to $\pm 115^o$)

3. Rear Region (For $\alpha_{sp} = \pm 115^o$ to $\pm 180^o$)

Forward Region

In this region there is only one figure for α_{sp}. Fig. 3.13 shows this graph in which one can easily see that the spanwise pressure distribution for a straked cylinder is same as that for a clean cylinder except for a very slight deviation at around 115 mm. which may due to the presence of strake at that location. In this case, actually, the stagnation pressure has been measured which remains unaffected by the presence

of helical strake. It has also been observed in the pressure distributions around the cylinder that the pressure distribution in the forward region of cylinder remains unchanged irrespective of the strake location.

Midriff Region

When the spanwise pressure distribution is measured in this region, the pressure distribution shows two local pressure peaks, one near 115 mm and the other near 400 mm, because the strake crosses the pressure ports at two locations near 115 mm and near 400 mm. These are shown in Fig. 3.7, 3.8, 3.10, 3.11, 3.12 and 3.14.

These figures are similar in the sense that each figure has pressure peaks at almost the same positions, near 115 mm and near 400 mm. These peaks are positive or negative depending upon the exact location of strake vis-a-vis the pressure port. If the strake is enhancing the separation of flow near the pressure port then the peak will be on the negative side and if the strake is blocking the flow near the pressure port then the peak will be on the positive side.

Rear Region

When the spanwise pressure distribution is been measured in the rear region of cylinder, the pressure distribution is found to be almost uniform throughout the span of the cylinder except for slight deviations at the two locations near 115 mm and 400 mm because of the presence of the strake at these two positions. These distributions are shown in Fig. 3.3, 3.4, 3.5, 3.6 and 3.9. The pressure is slightly higher in all the figures at all the spanwise locations. This is also verified from the radial pressure distribution in which it has been seen that the pressure distribution

in the rear region of cylinder remains unchanged irrespective of the strake location. Strake only causes a slightly higher pressure in rear region.

3.3 Discussion

Helical strake basically makes the cylinder geometry three dimensional particularly in the spanwise direction. As a result no two spanwise stations within one pitch of helical strake show identical mean flow distribution unlike the clean cylinder where all spanwise stations away from the tunnel walls show identical mean flow distribution.

The effect of helical strake depends on the angle between the helical strake location at mid-span and the flow direction (α_{hs}). Based on this three regions can be identified from the present data. The forward and rear regions show identical effects. These regions show a slightly higher pressure in midriff and rear regions of cylinder. The midriff region shows local pressure peaks near the strake location and also a slight increase in pressure in the rear and the midriff regions. The pressure peaks are found due to the excessive separation by strake.

Spanwise pressure distribution is seen clearly by dividing the curves with the help of the angle α_{sp}. Here the forward region shows minimal effect and the midriff region shows maximum effect. The effect shown by rear region is the intermediate effect. It is different from the distributions for the forward region because it shows a slightly higher pressure at all the spanwise stations.

The present data shows the highly asymmetric nature of mean flow field both in the spanwise direction as well as upward and downward/forward and backward regions at each span.

From applied point of view helical strakes are known to suppress vortex shedding which is the fluctuating flow field. However the present experiment show that mean flow field is also disturbed significantly by the presence of strake. The total picture will require the measurement of fluctuating quantities in the wake region which can be a subject of further study.

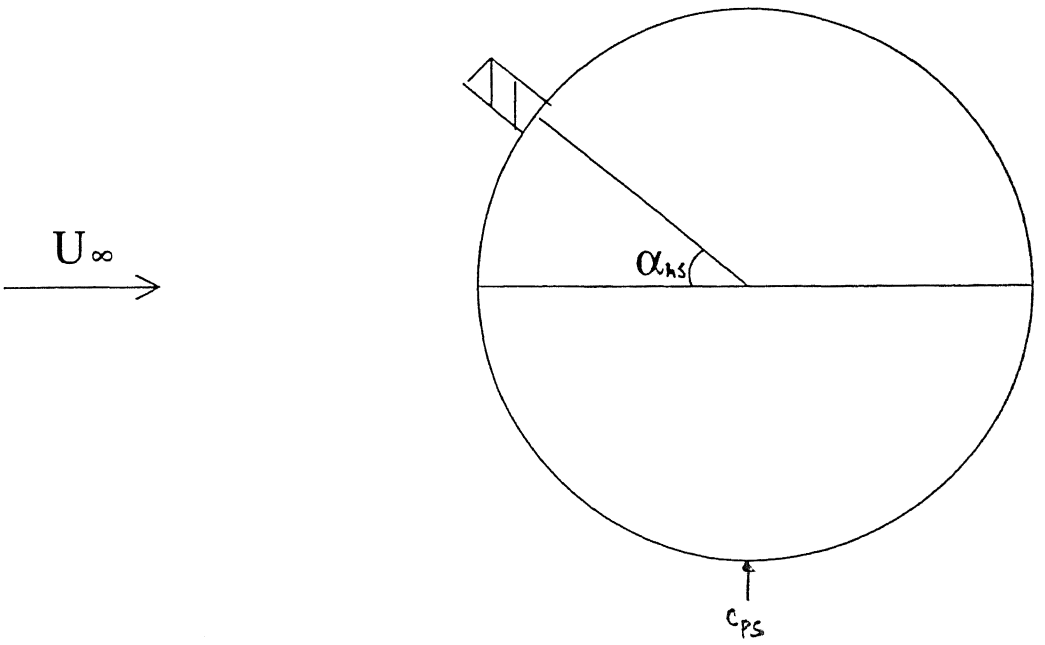

Figure 3.1: Figure Showing Strake Location at Mid-span w.r.t Flow Direction

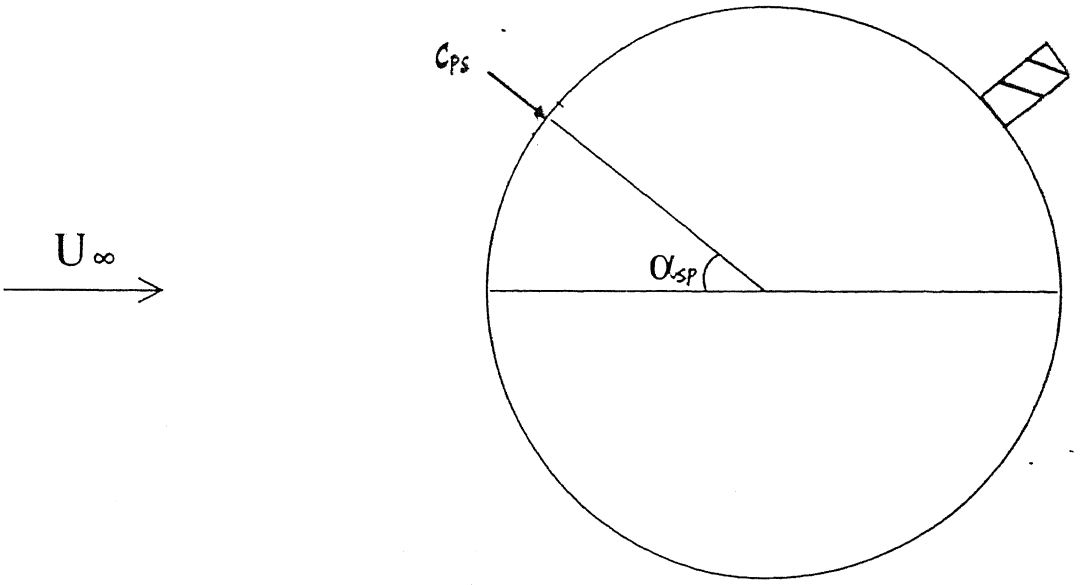

Figure 3.2: Figure Showing Location of Radial Station, at Which the Spanwise Distribution of Pressure is Measured, w.r.t Flow Direction

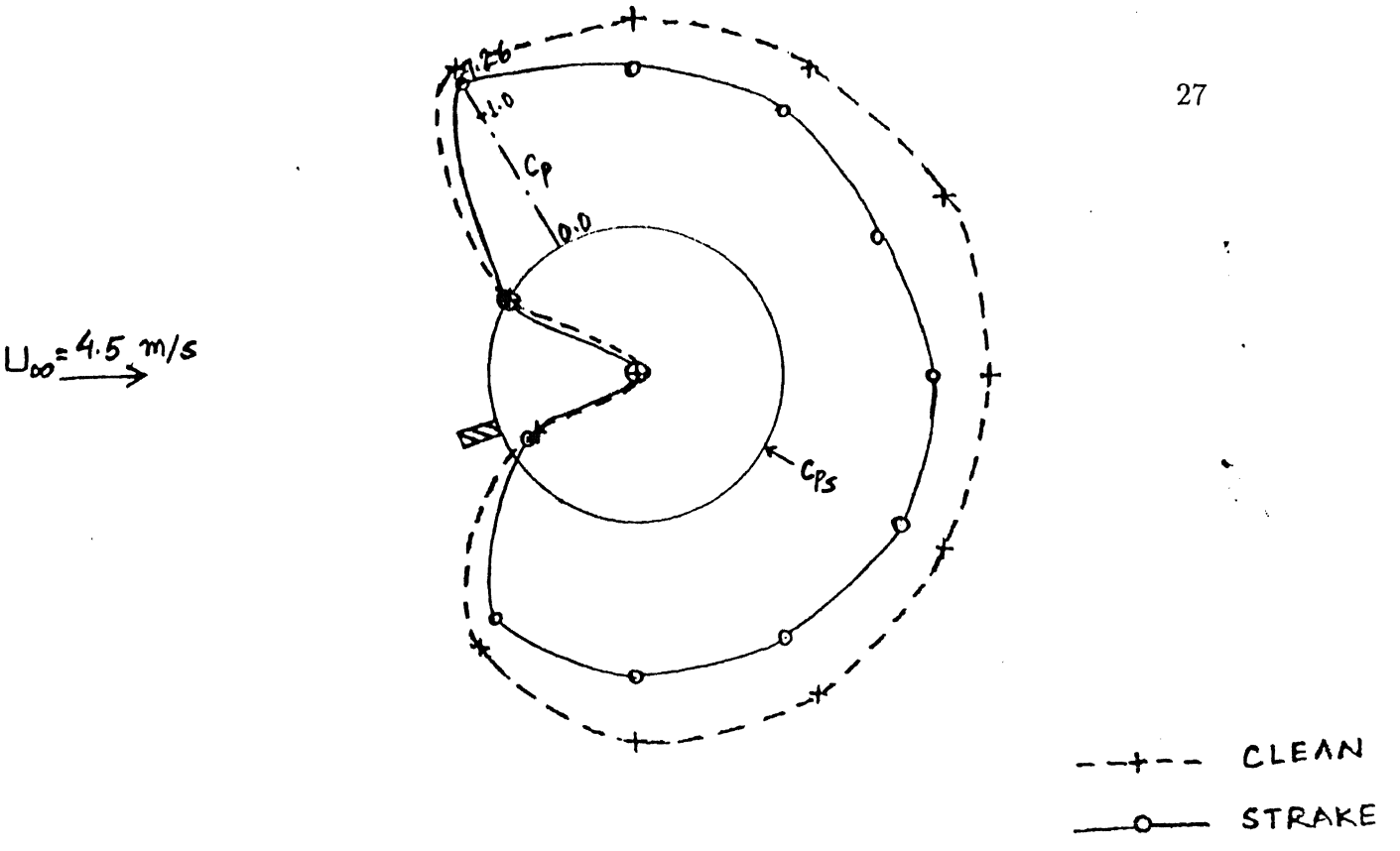

Radial Pressure Distribution

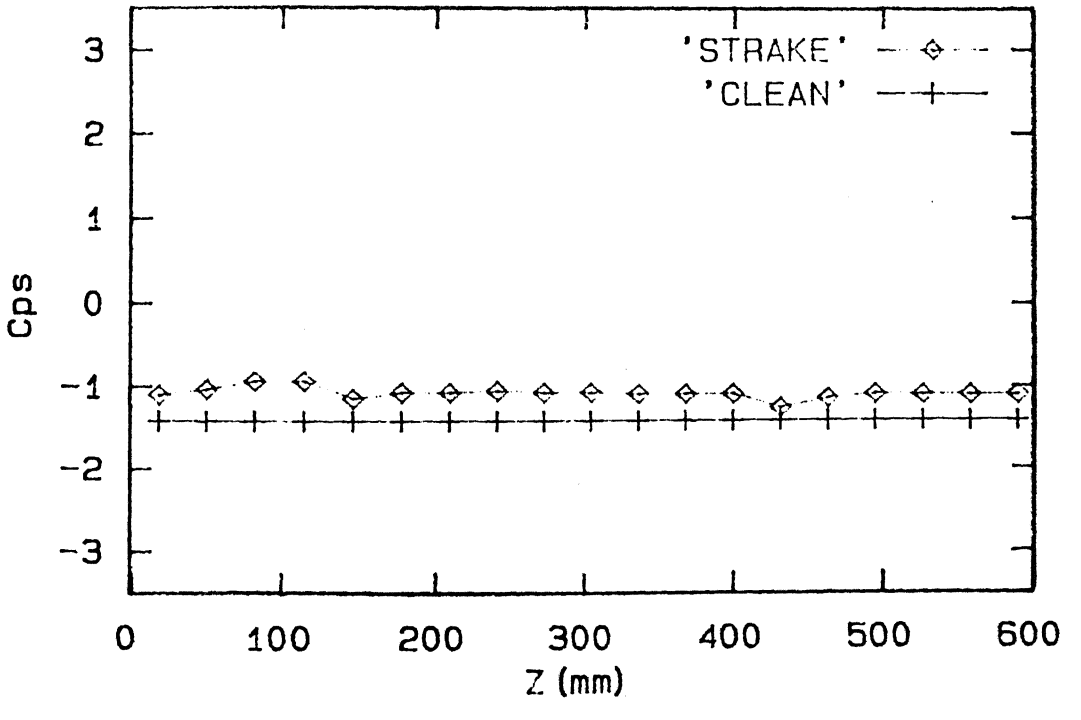

Spanwise Pressure Distribution

Figure 3.3: Pressure Distribution for $\alpha_{sp} = -150^{o}$ and $U_{\infty} = 4.5$ m/s

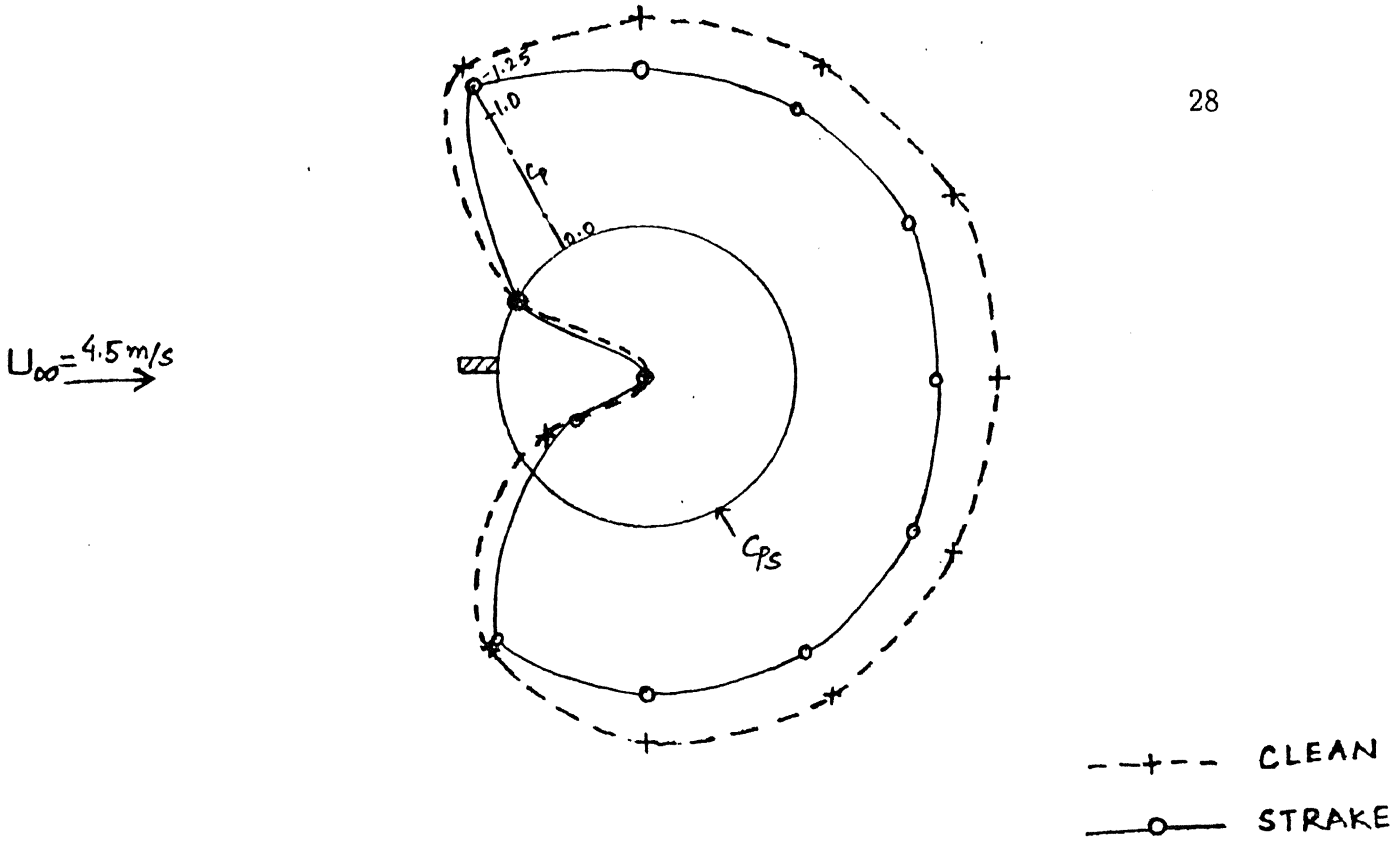

Radial Pressure Distribution

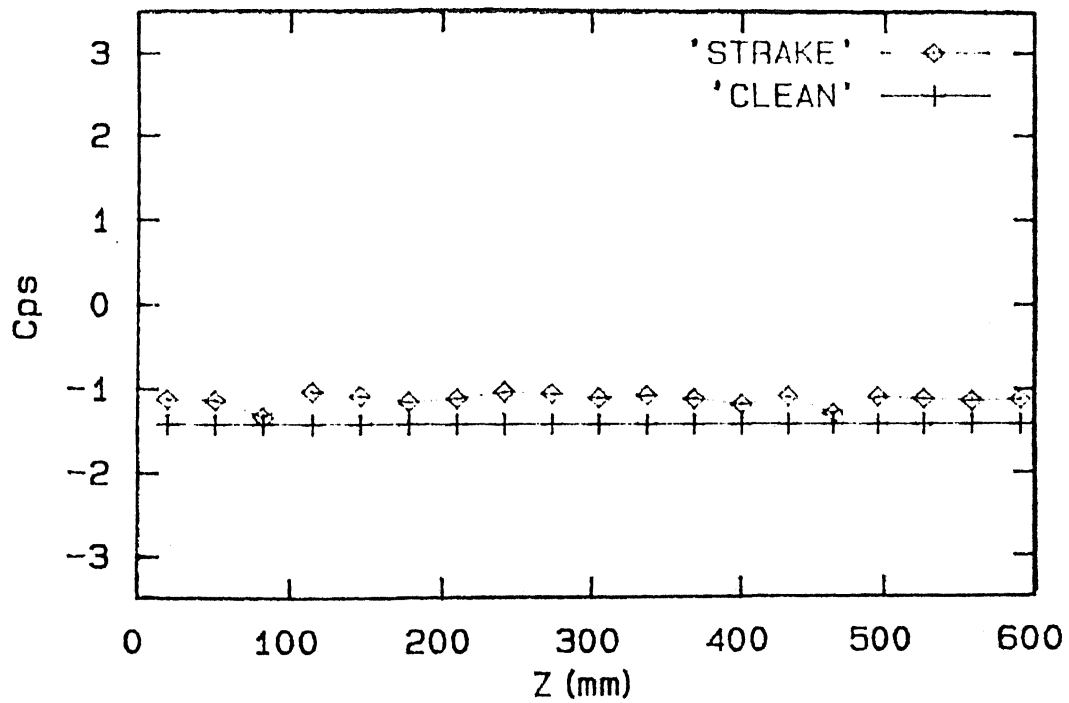

Spanwise Pressure Distribution

Figure 3.4: Pressure Distribution for $\alpha_{sp} = -120°$ and $U_\infty = 4.5$ m/s

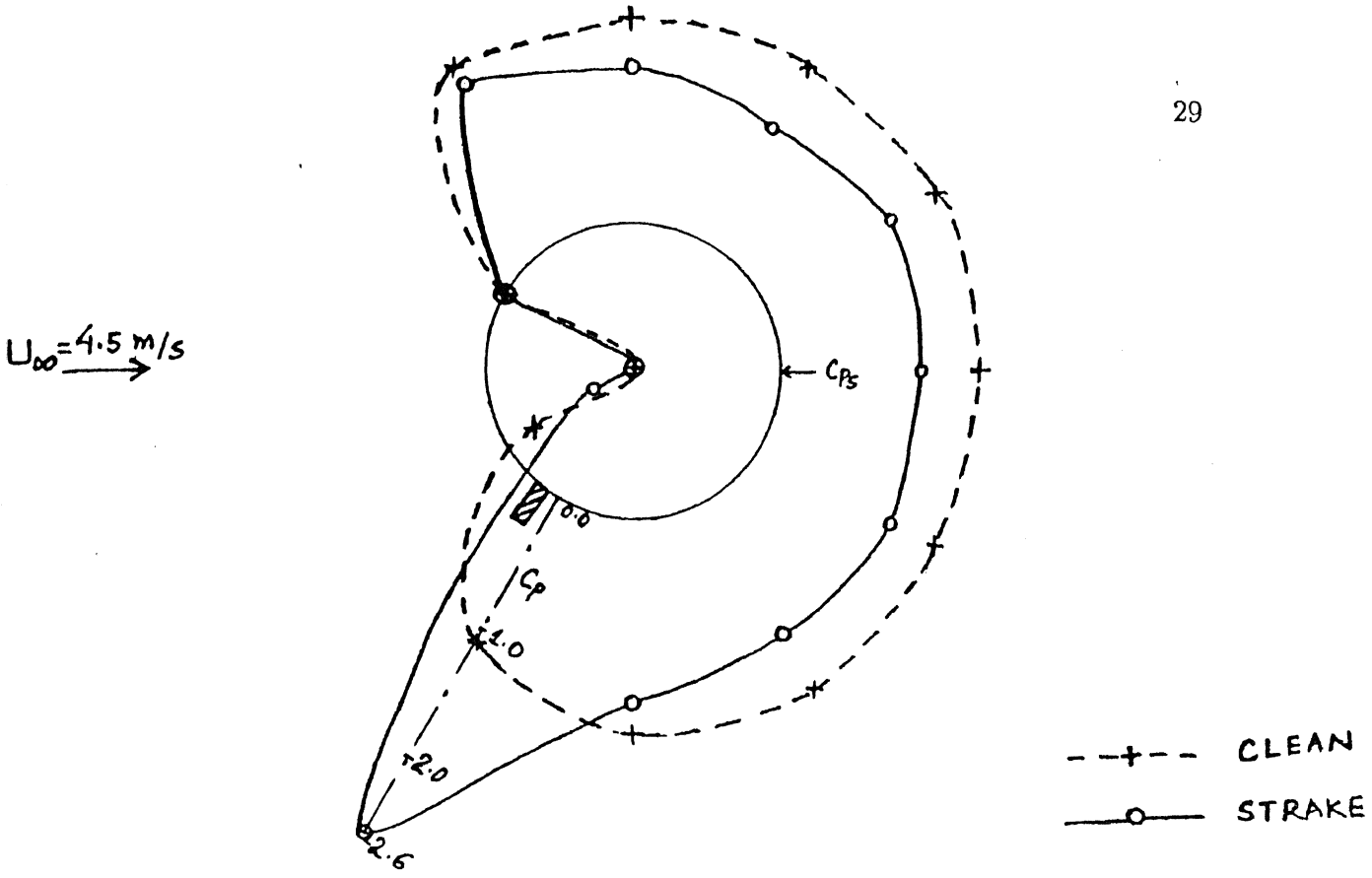

Radial Pressure Distribution

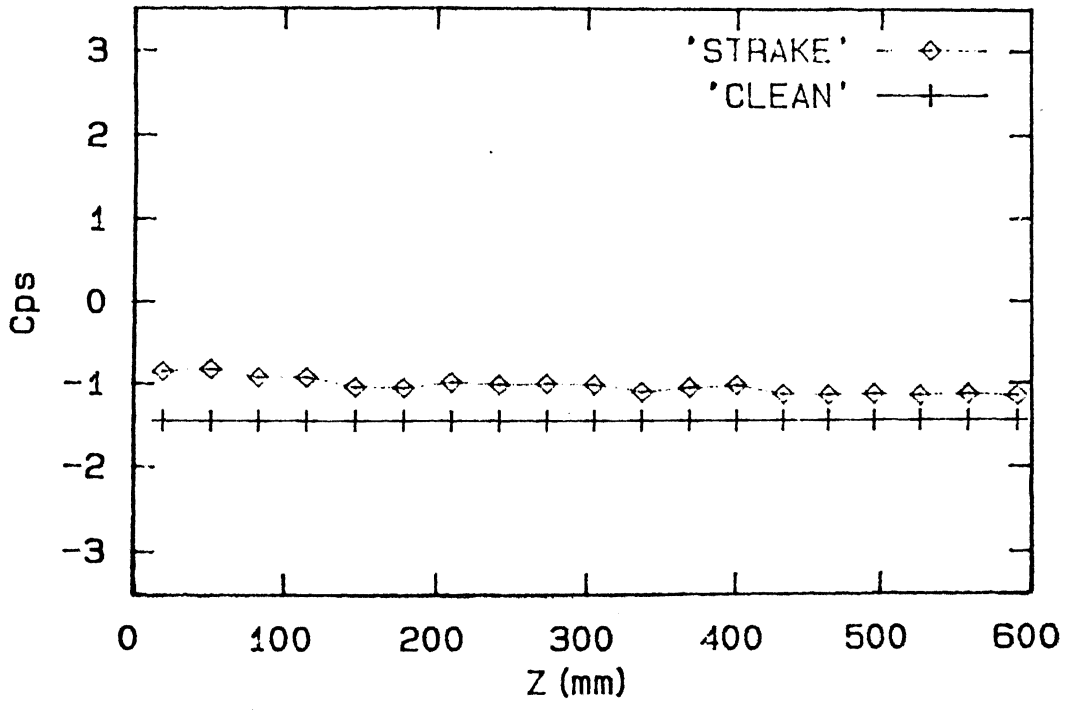

Spanwise Pressure Distribution

Figure 3.5: Pressure Distribution for $\alpha_{sp} = 180°$ and $U_\infty = 4.5$ m/s

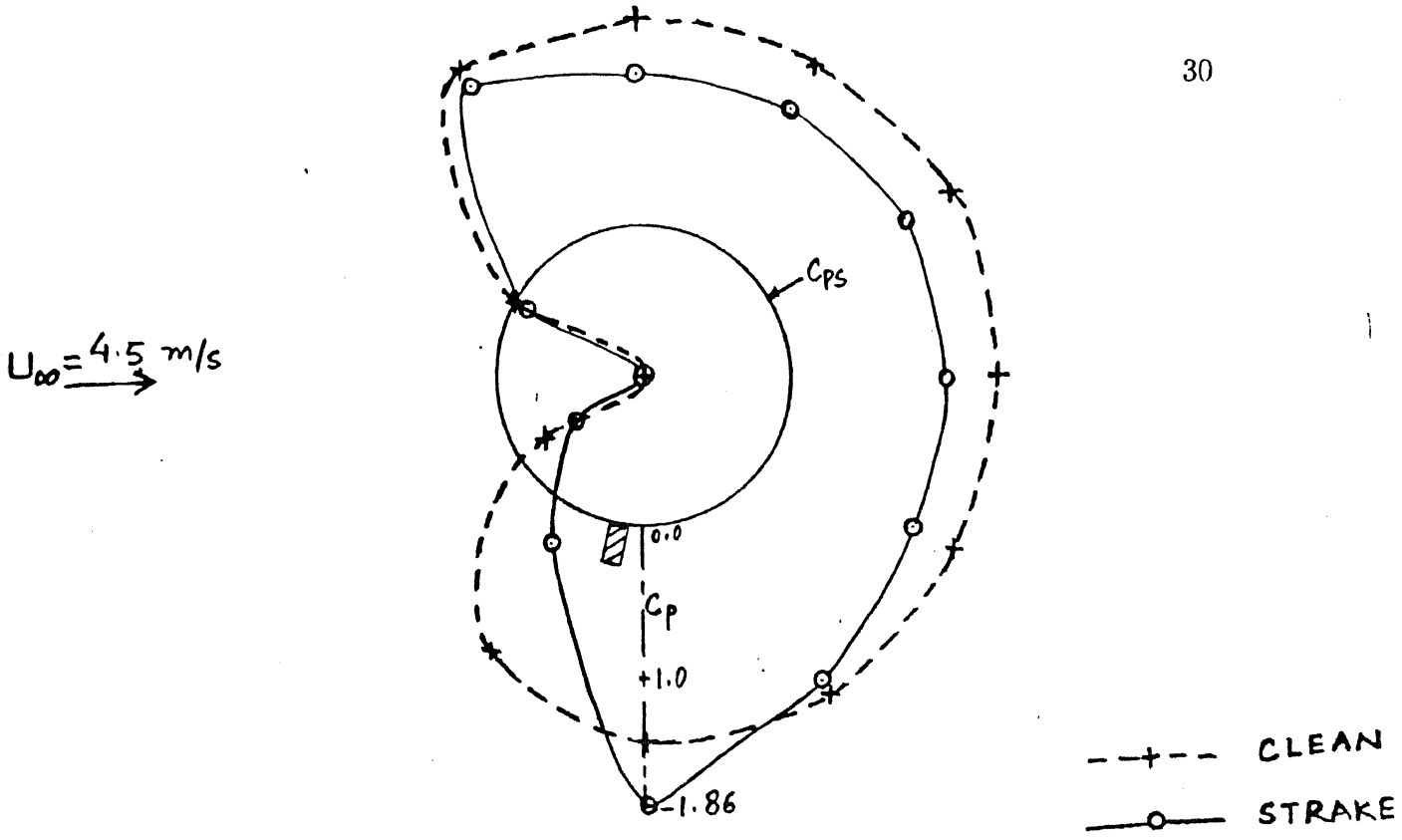

Radial Pressure Distribution

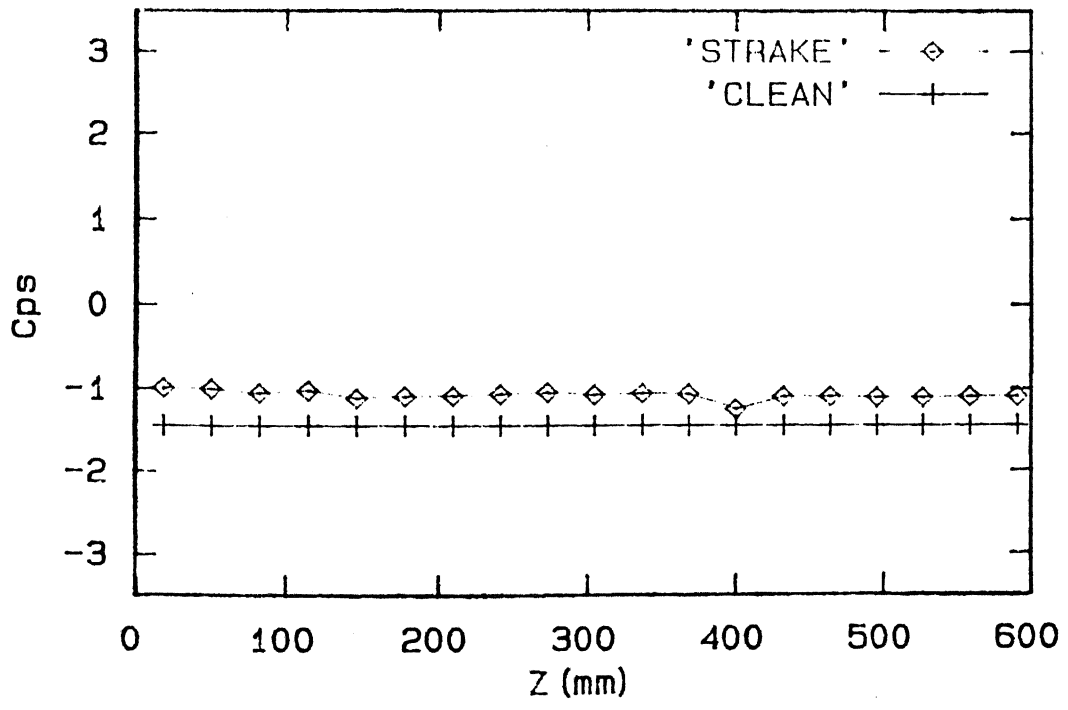

Spanwise Pressure Distribution

Figure 3.6: Pressure Distribution for $\alpha_{sp} = 150^o$ and $U_\infty = 4.5$ m/s

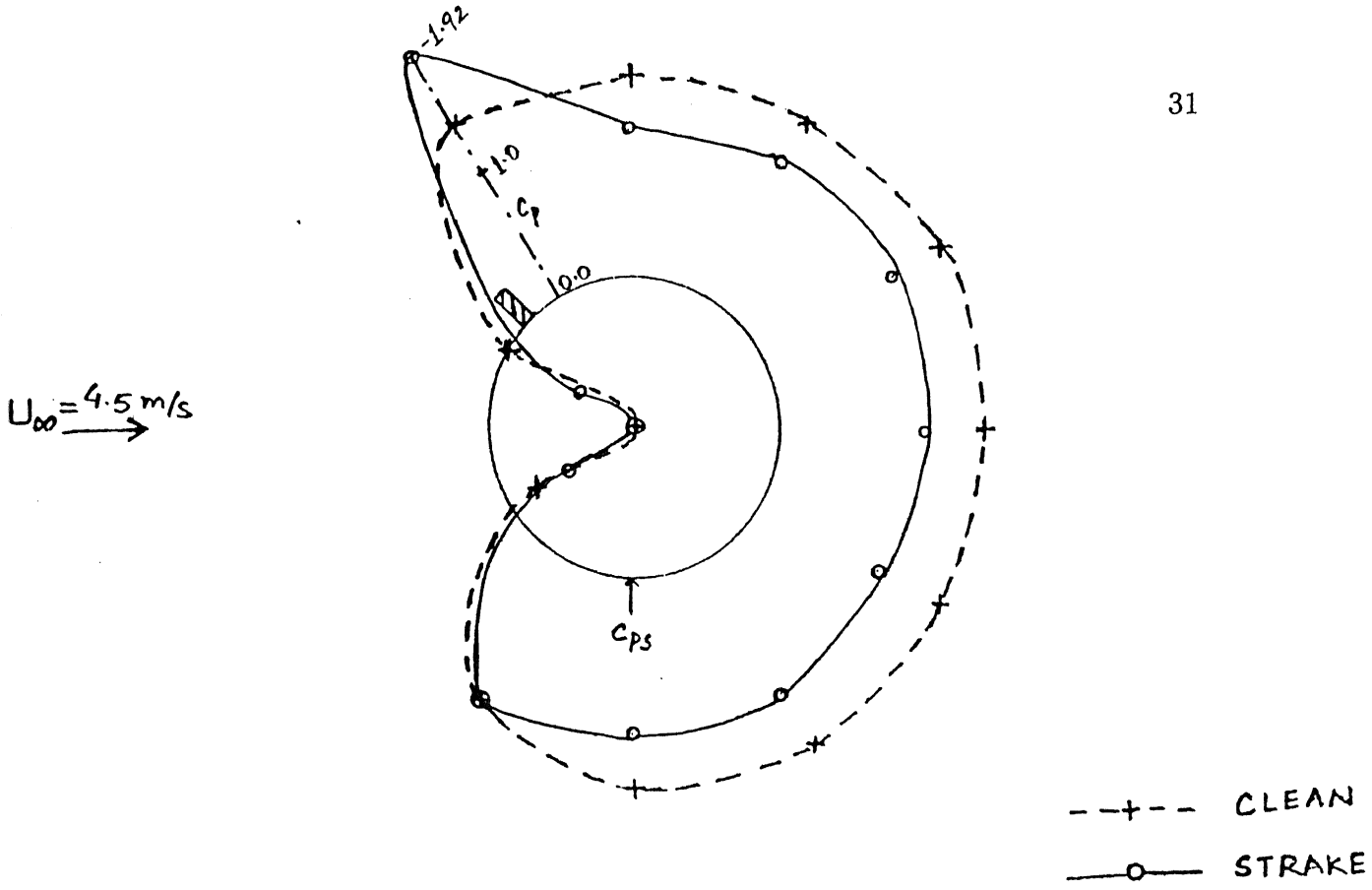

Radial Pressure Distribution

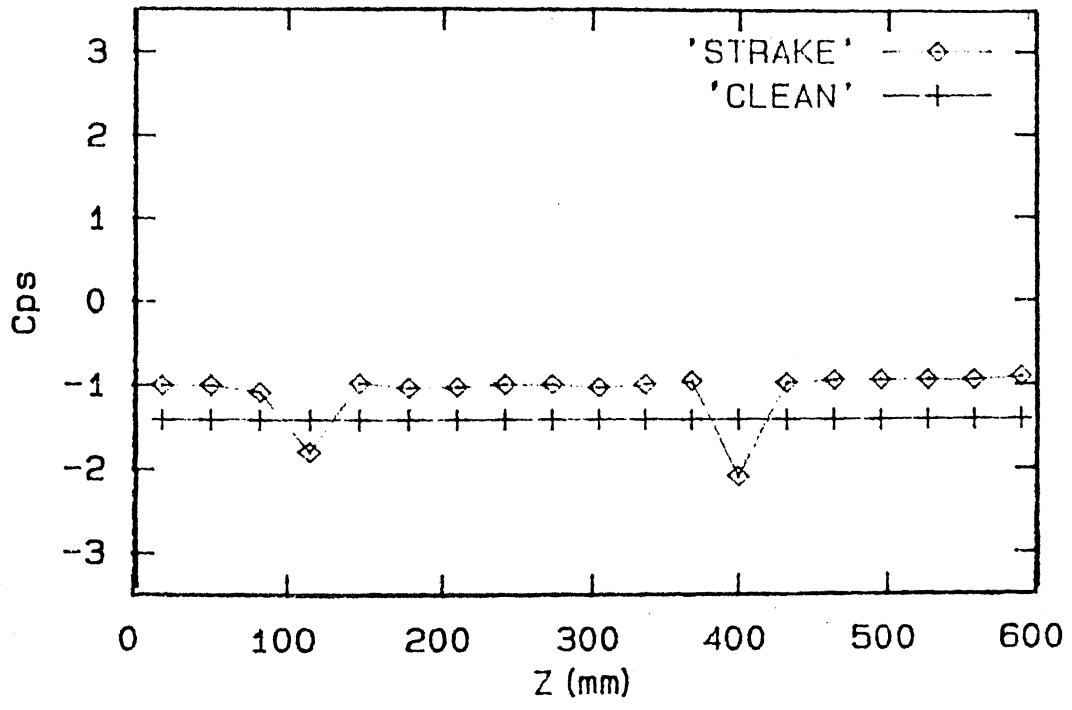

Spanwise Pressure Distribution

Figure 3.7: Pressure Distribution for $\alpha_{sp} = -90^o$ and $U_\infty = 4.5$ m/s

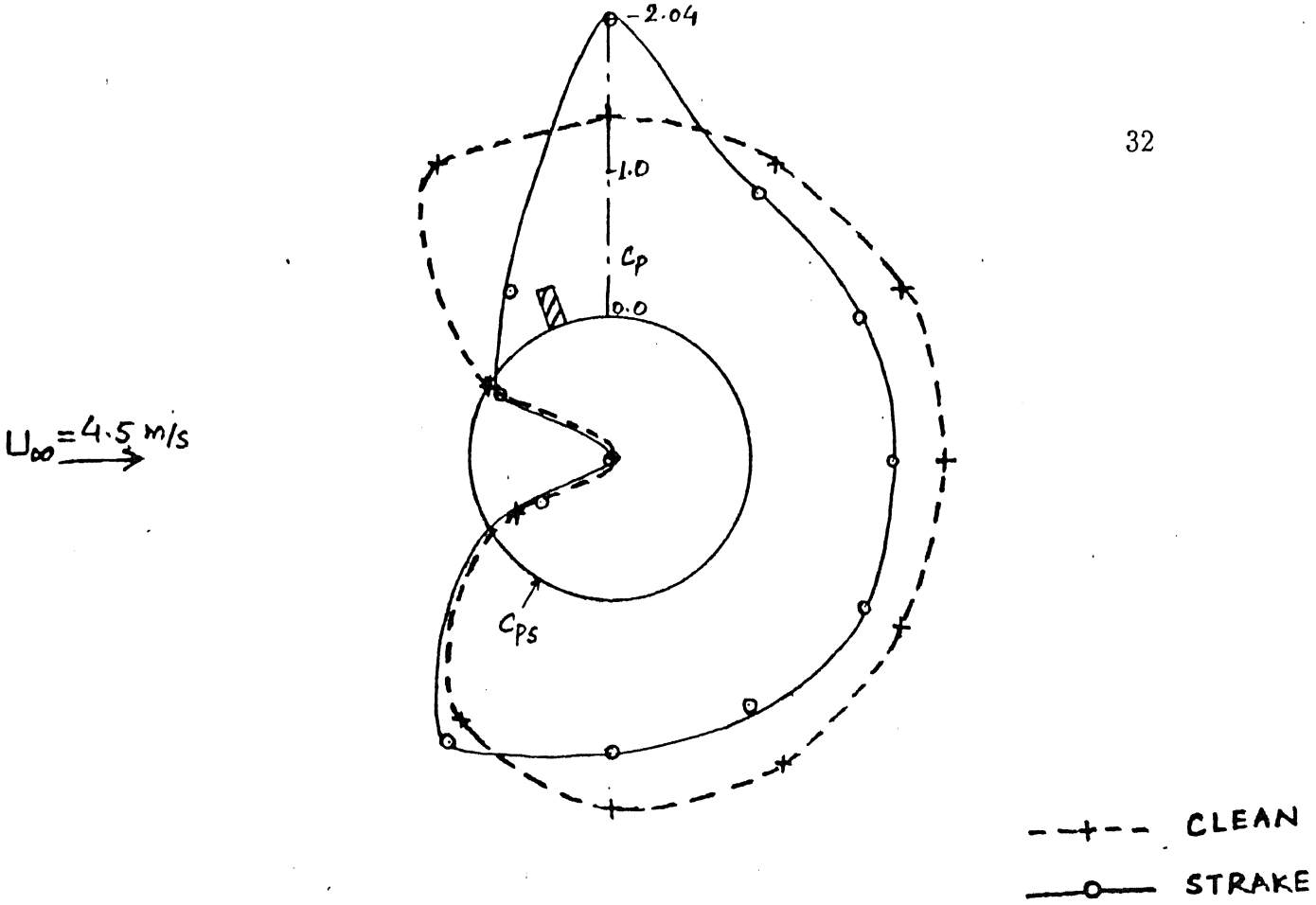

Radial Pressure Distribution

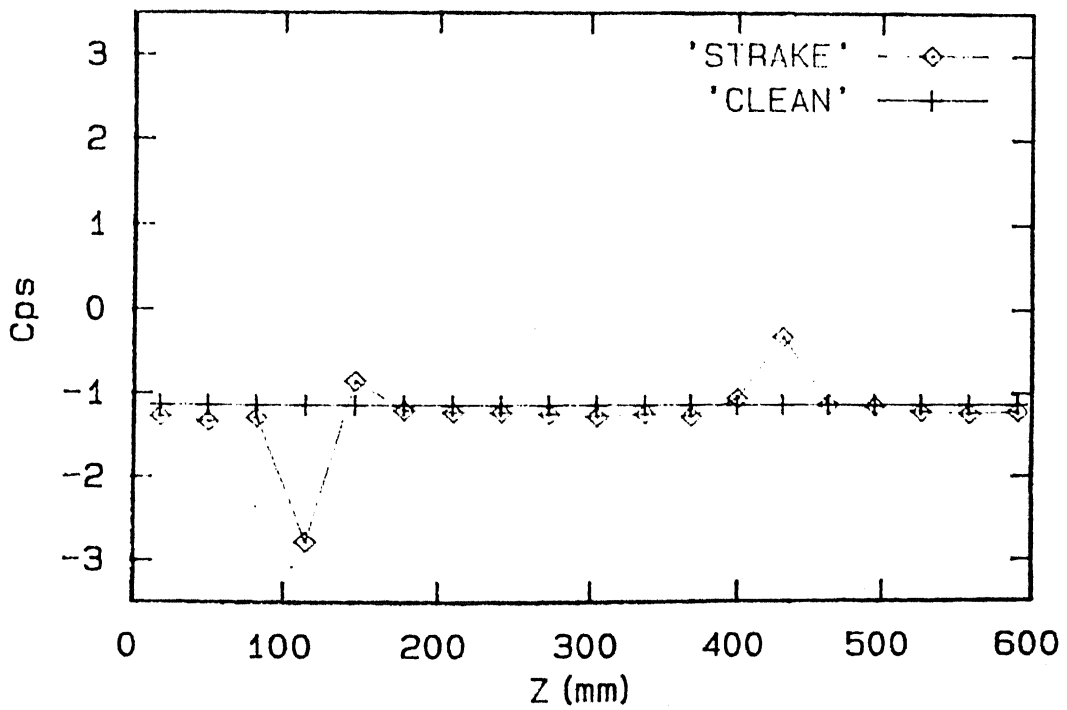

Spanwise Pressure Distribution

Figure 3.8: Pressure Distribution for $\alpha_{sp} = -60^{o}$ and $U_{\infty} = 4.5$ m/s

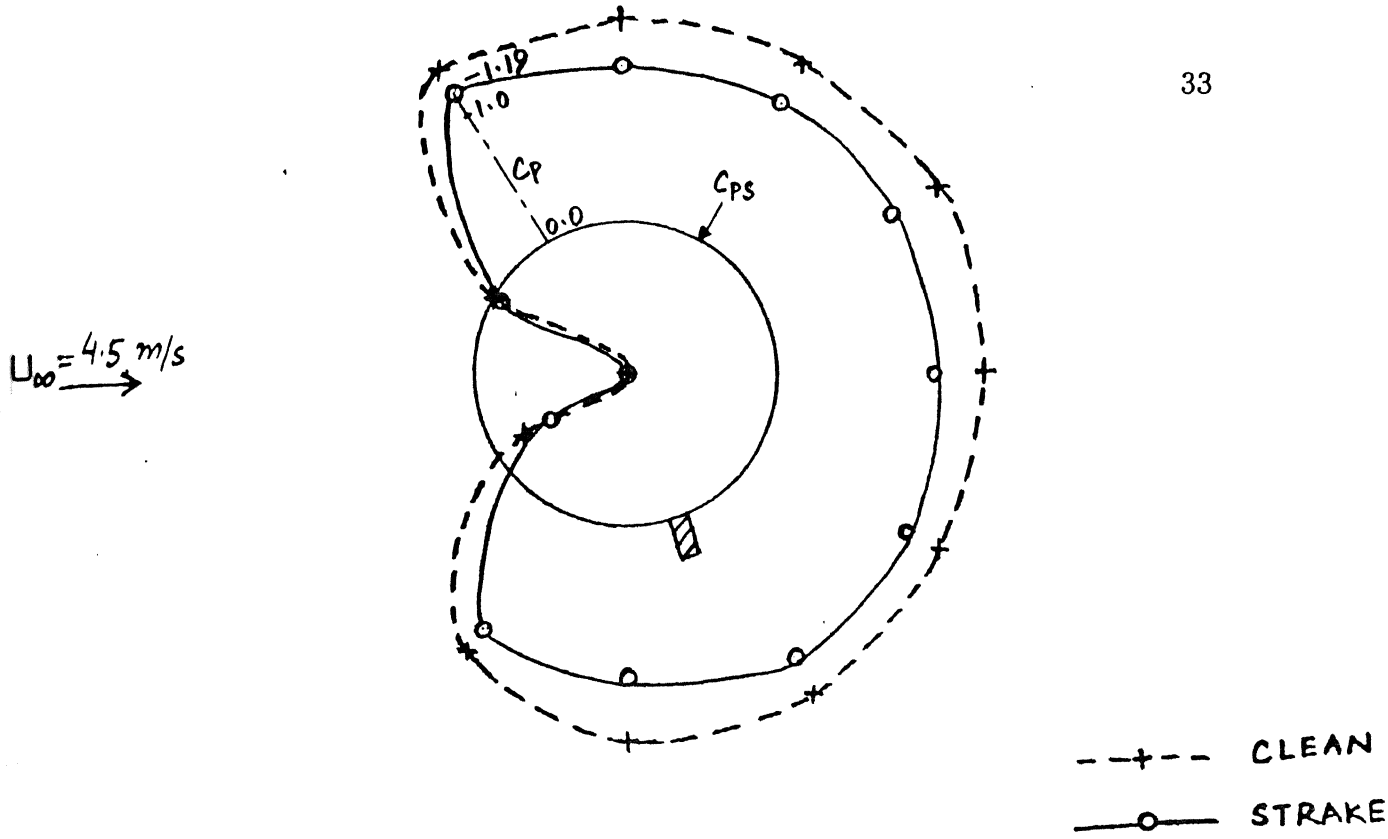

Radial Pressure Distribution

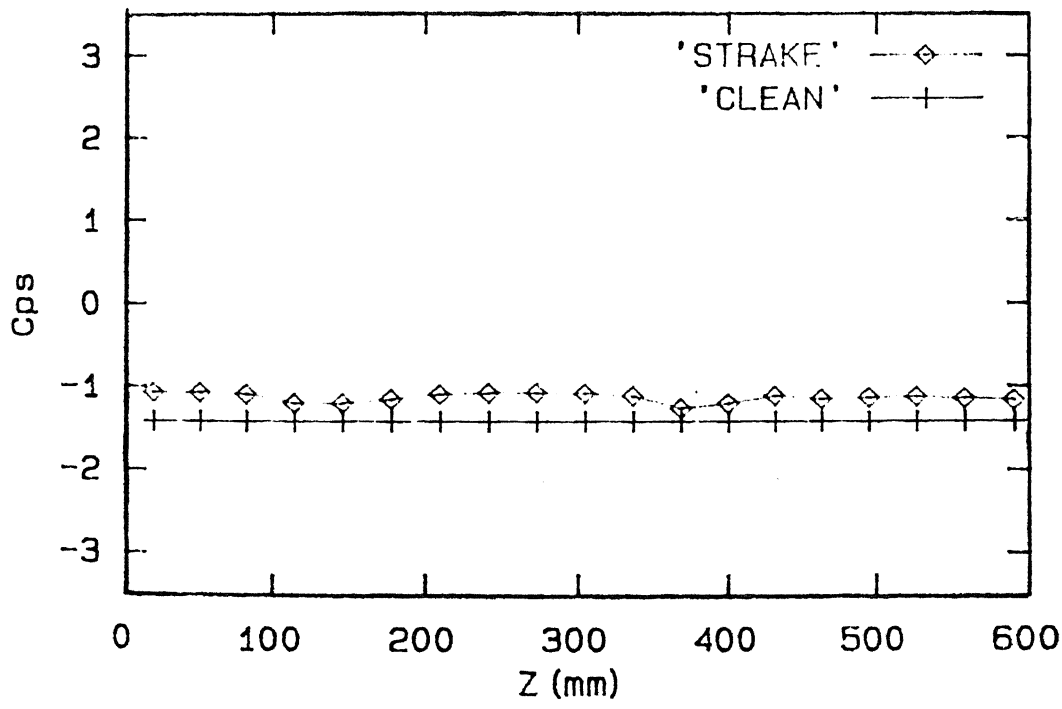

Spanwise Pressure Distribution

Figure 3.9: Pressure Distribution for $\alpha_{sp} = 120^{\circ}$ and $U_{\infty} = 4.5$ m/s

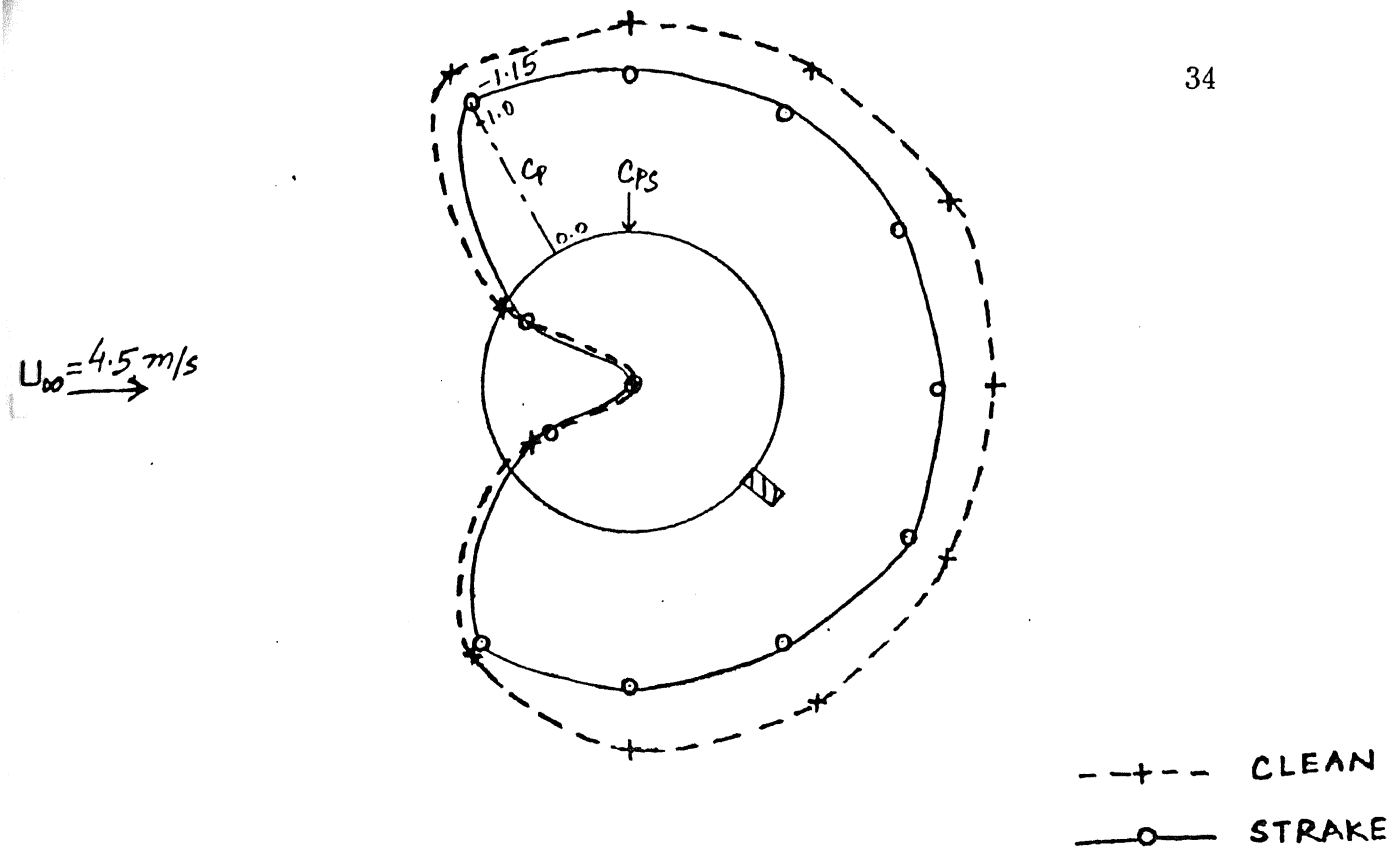

Radial Pressure Distribution

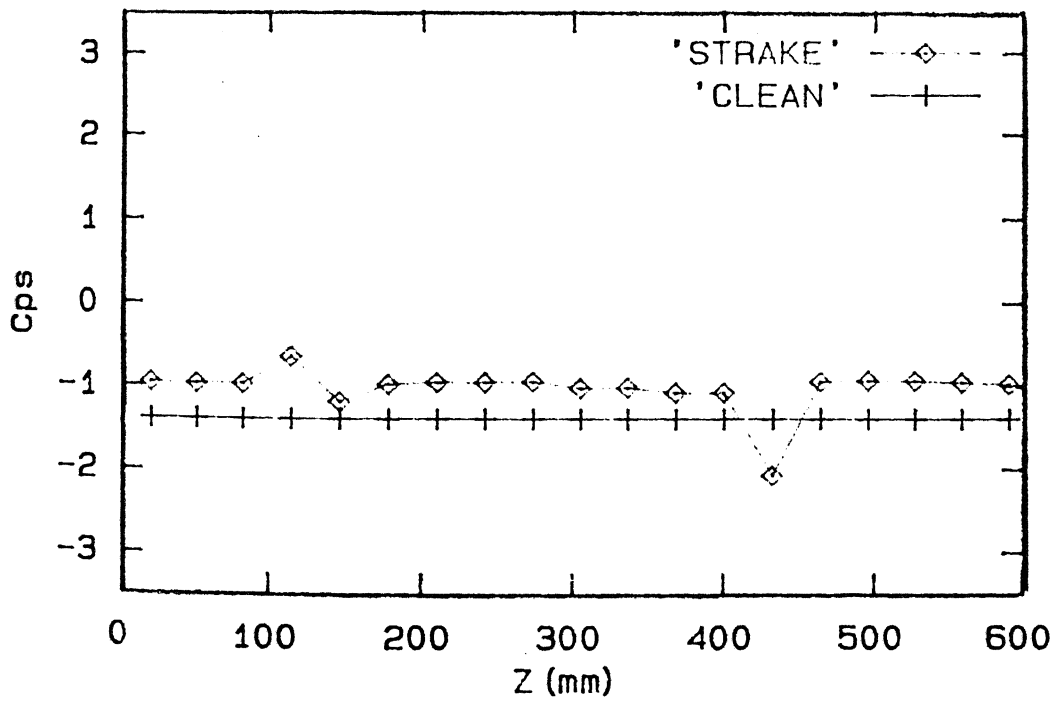

Spanwise Pressure Distribution

Figure 3.10: Pressure Distribution for $\alpha_{sp} = 90°$ and $U_\infty = 4.5$ m/s

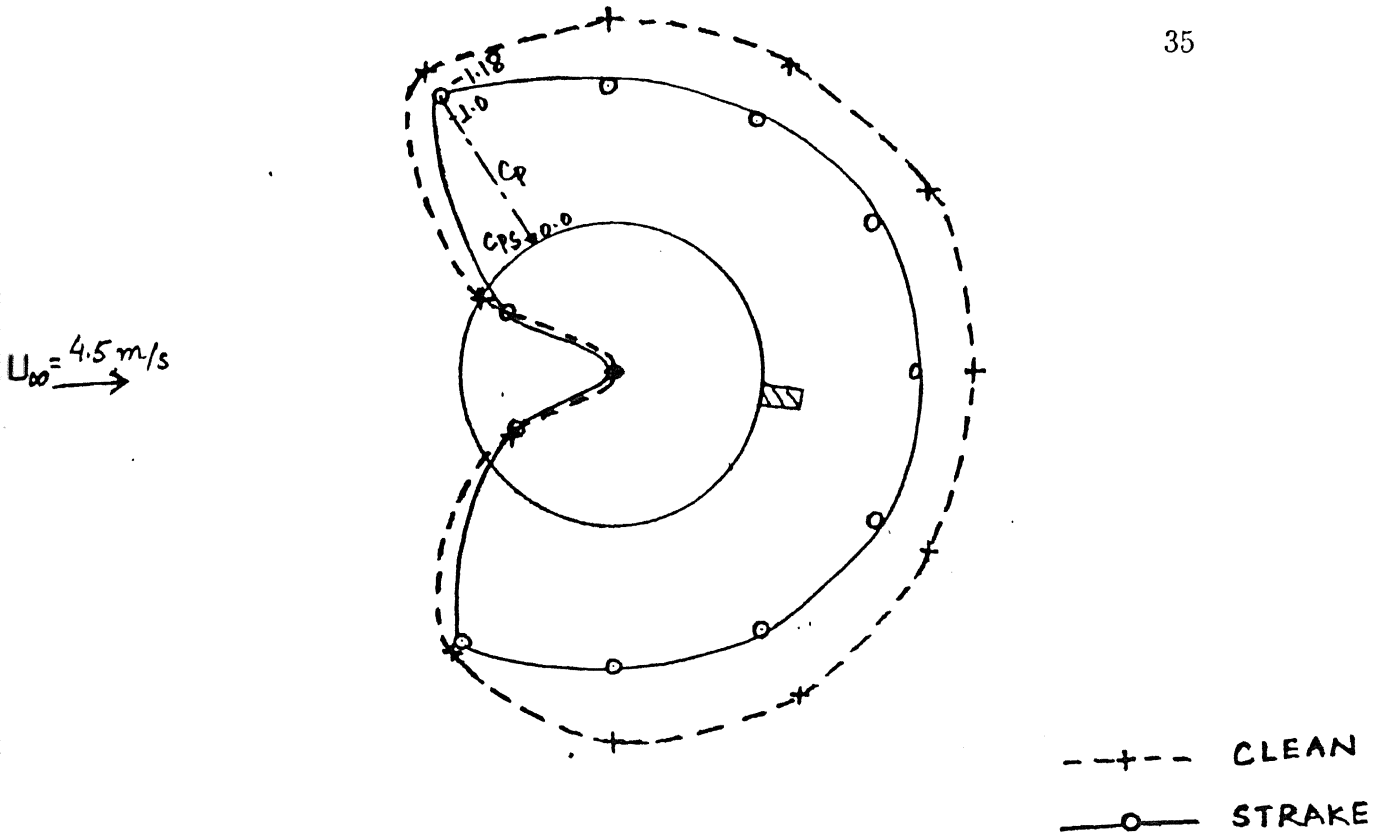

Radial Pressure Distribution

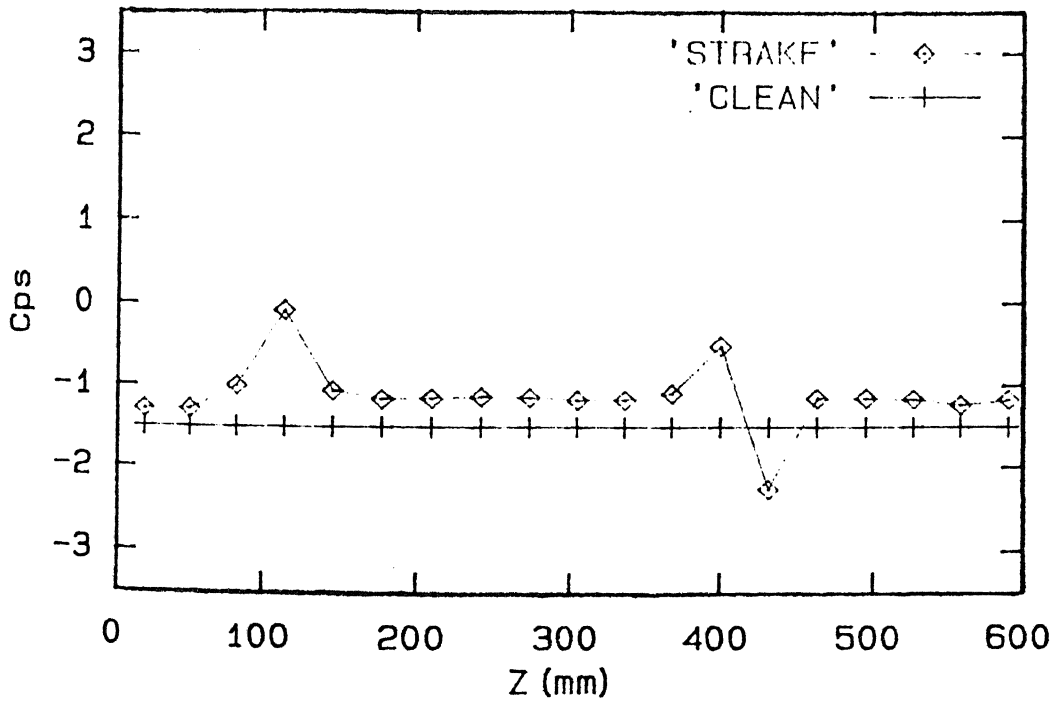

Spanwise Pressure Distribution

Figure 3.11: Pressure Distribution for $\alpha_{sp} = 60°$ and $U_\infty = 4.5$ m/s

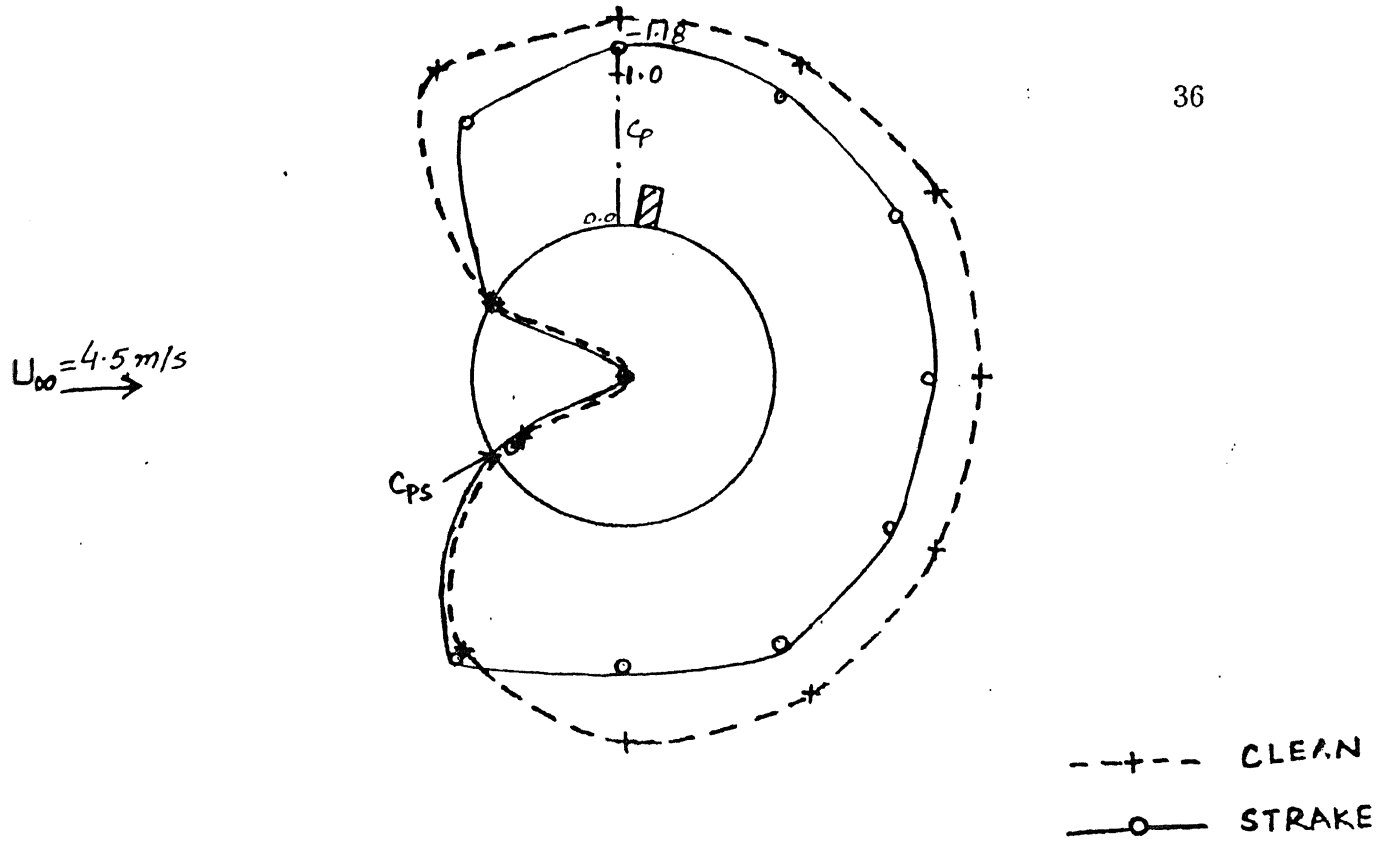

Radial Pressure Distribution

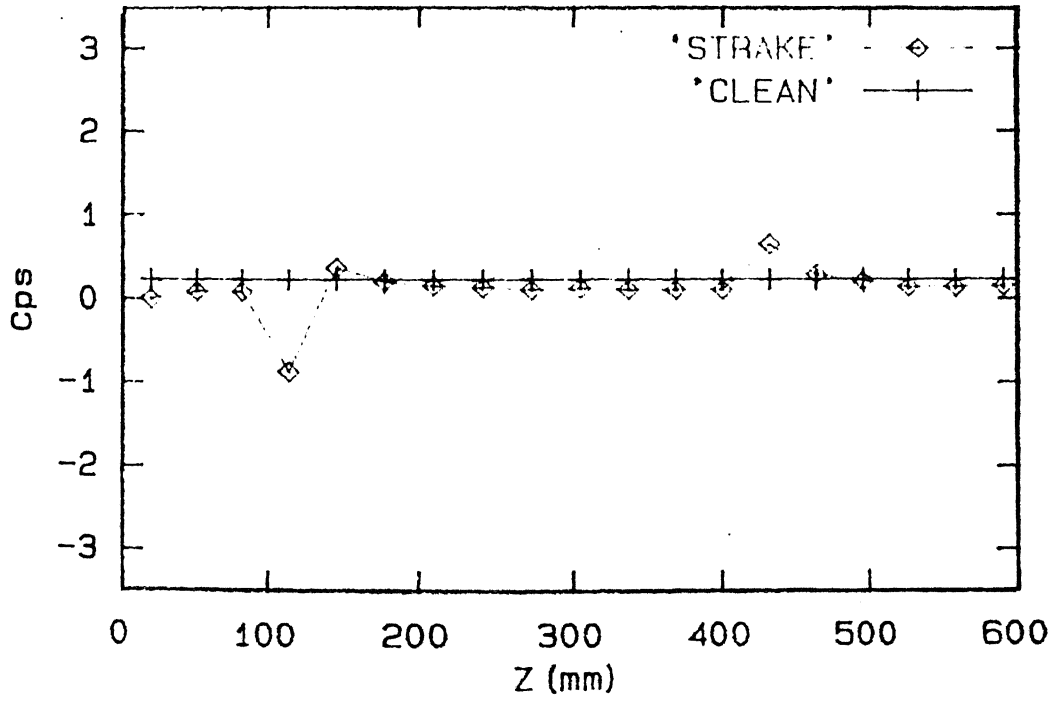

Spanwise Pressure Distribution

Figure 3.12: Pressure Distribution for $\alpha_{sp} = -30°$ and $U_\infty = 4.5$ m/s

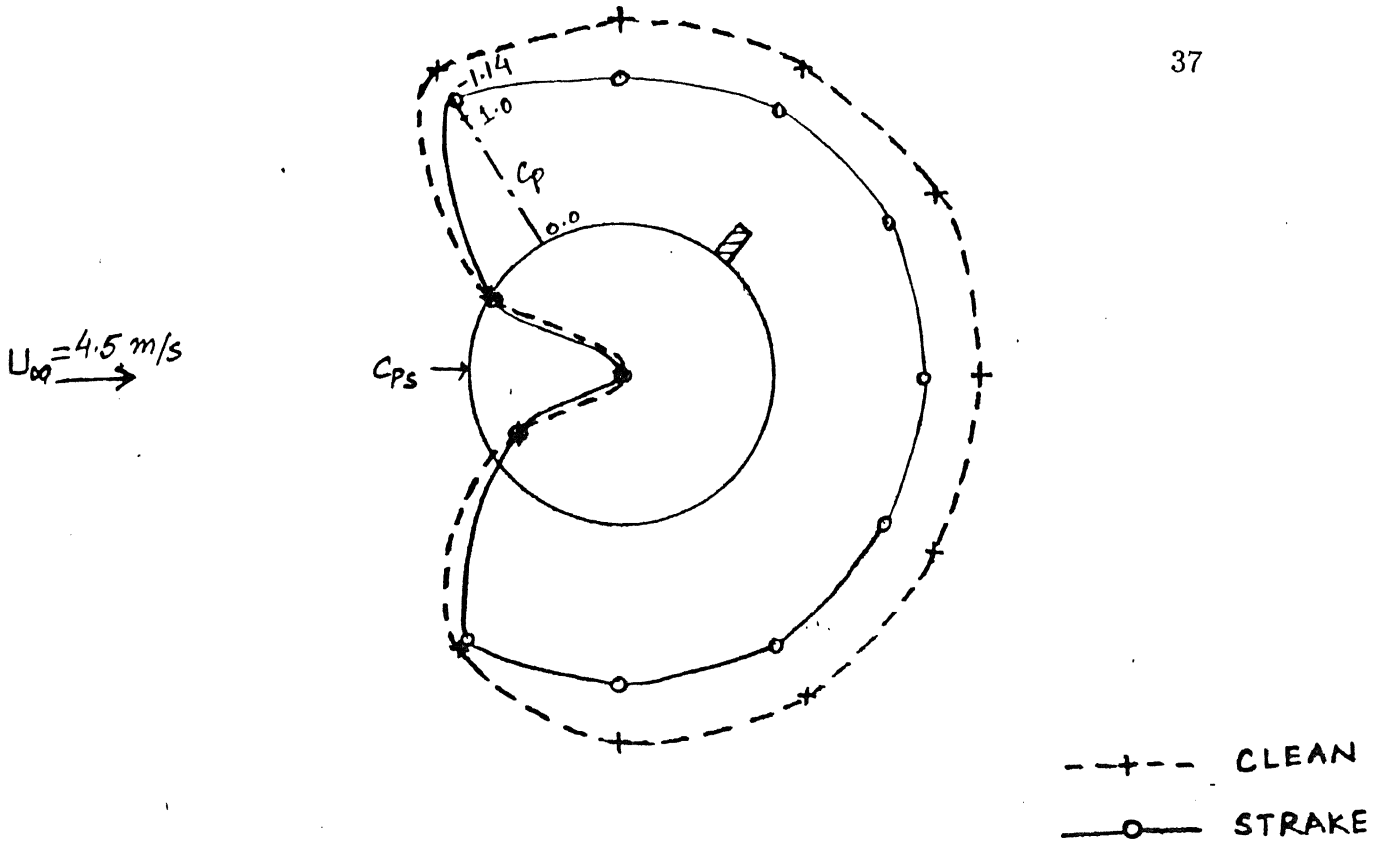

Radial Pressure Distribution

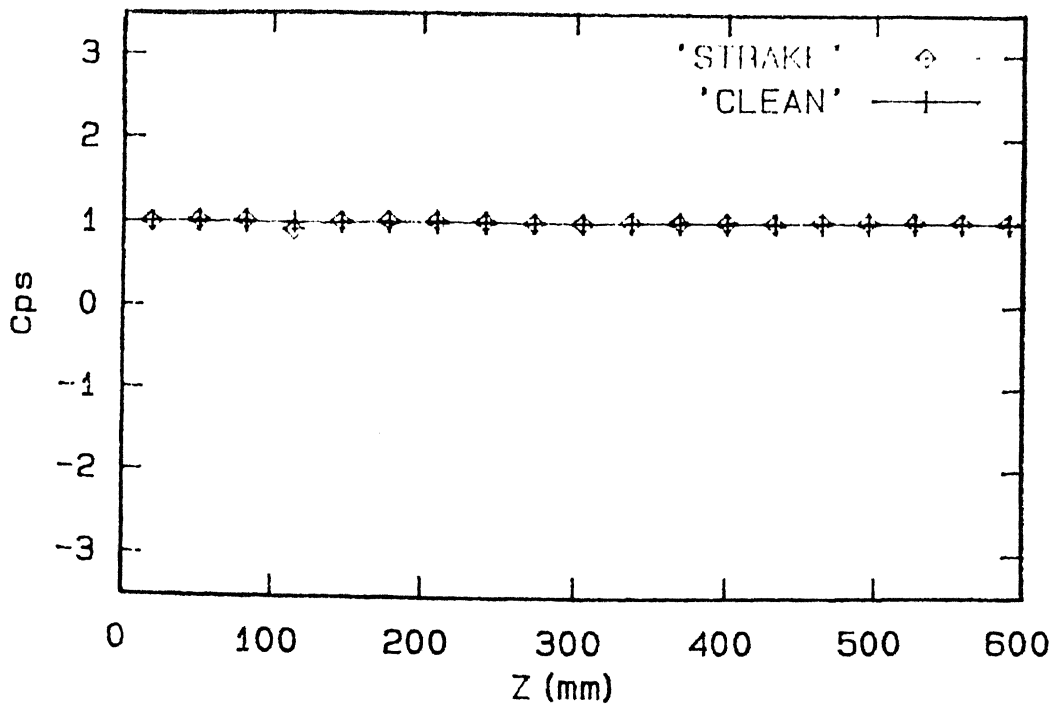

Spanwise Pressure Distribution

Figure 3.13: Pressure Distribution for $\alpha_{sp} = 0°$ and $U_\infty = 4.5$ m/s

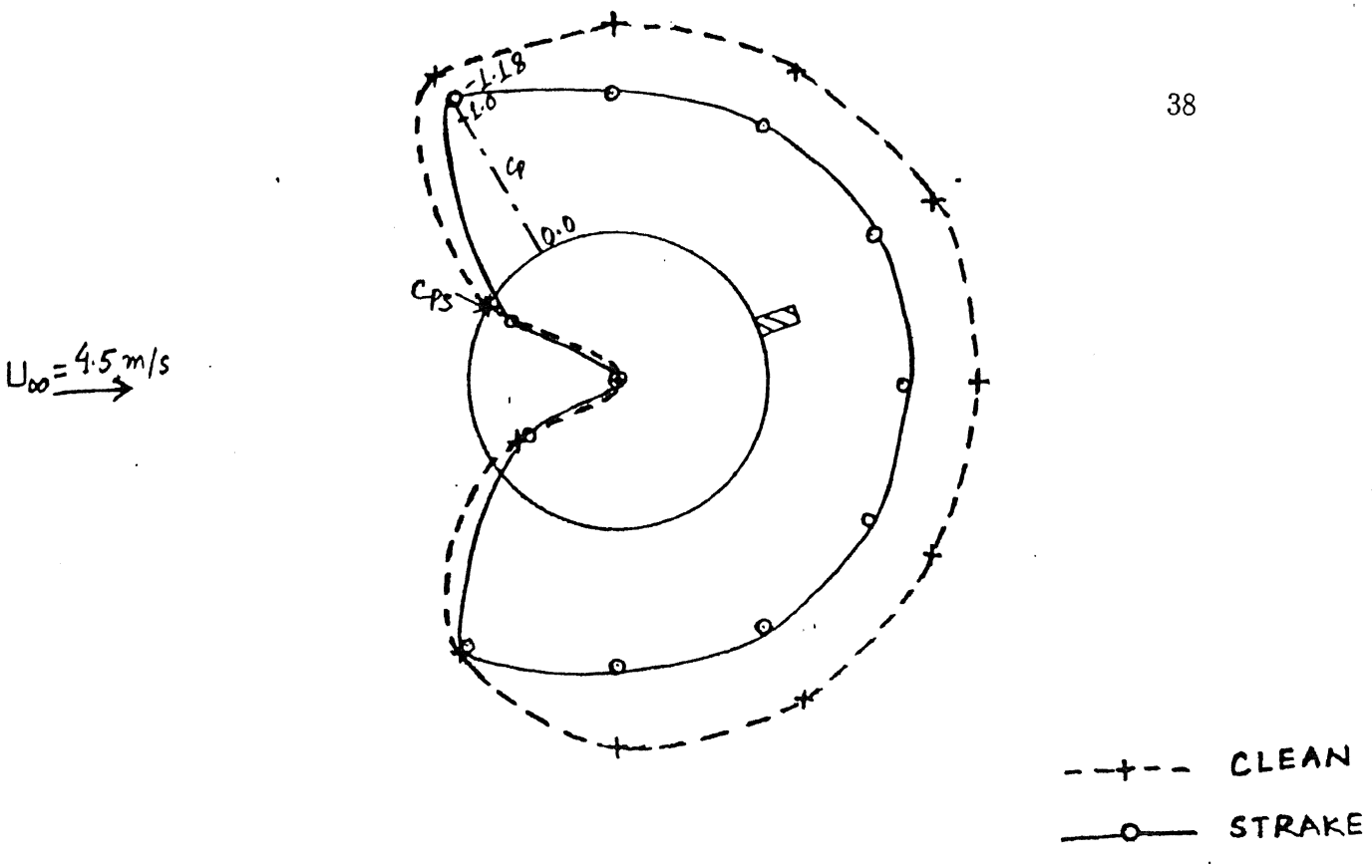

Radial Pressure Distribution

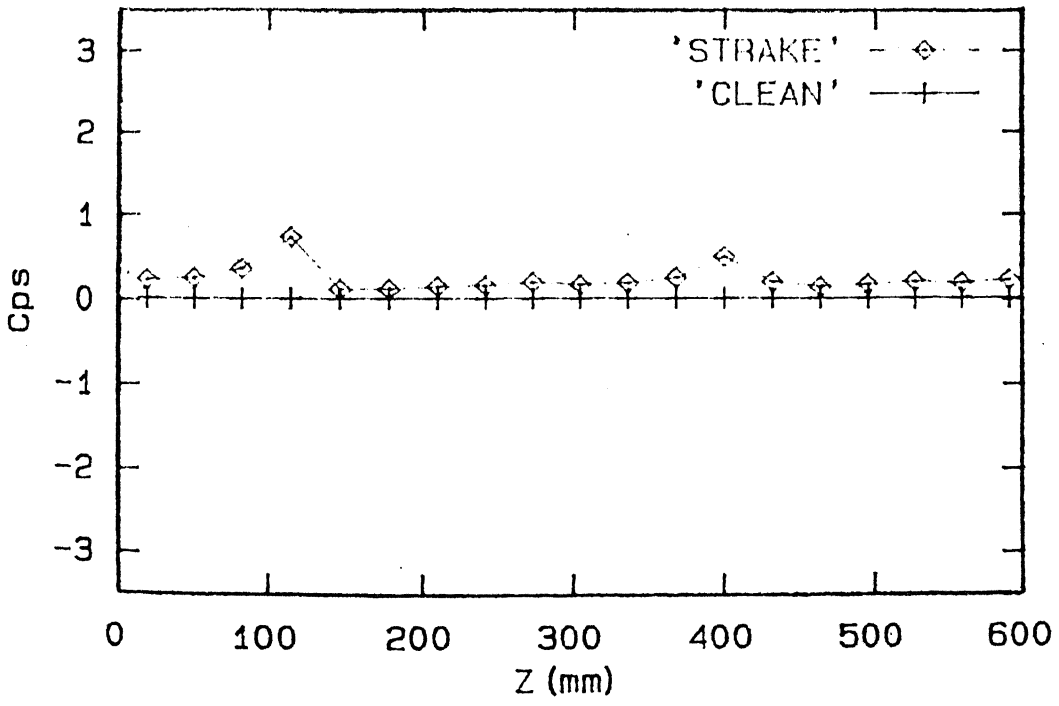

Spanwise Pressure Distribution

Figure 3.14: Pressure Distribution for $\alpha_{sp} = 30^o$ and $U_\infty = 4.5$ m/s

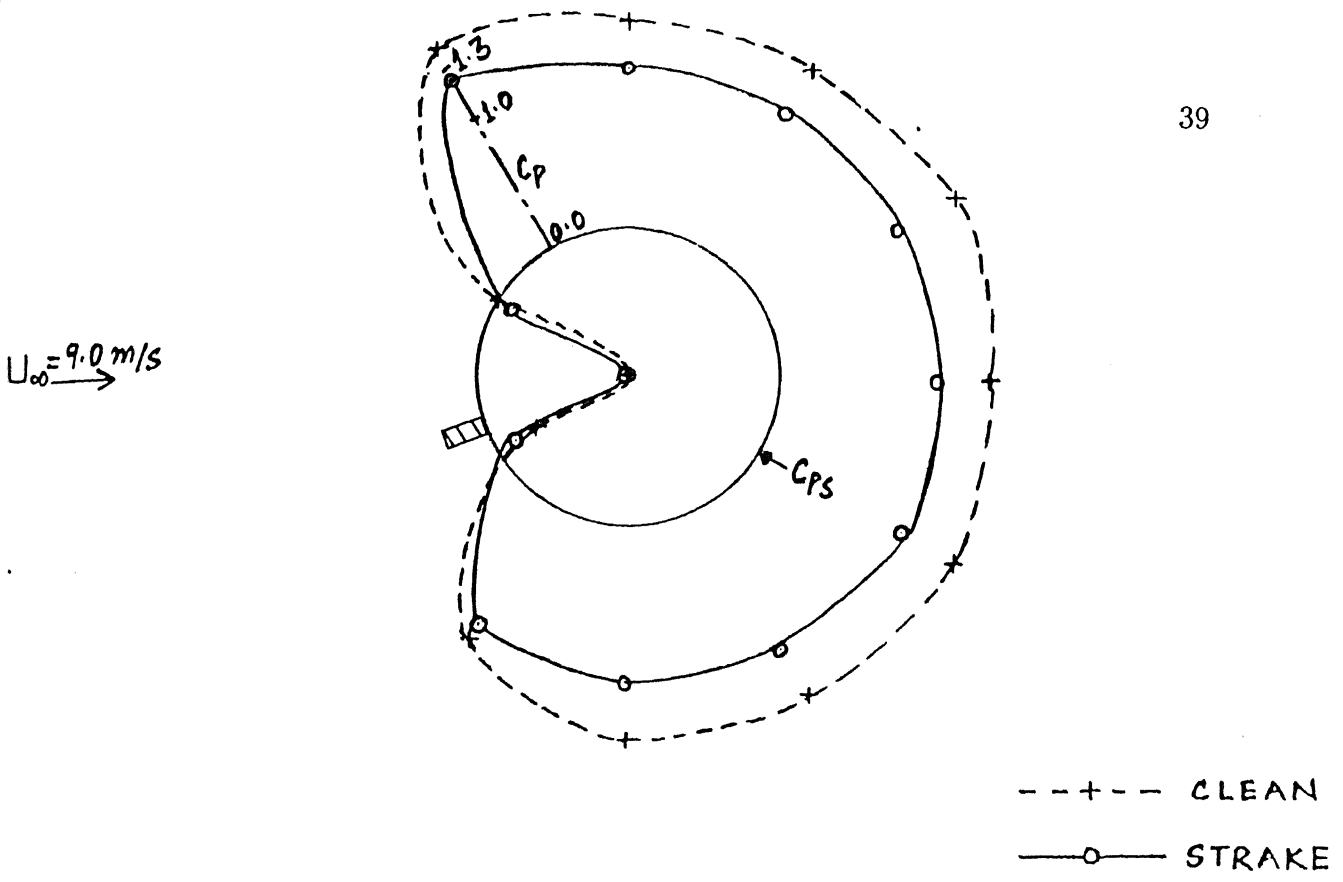

Radial Pressure Distribution

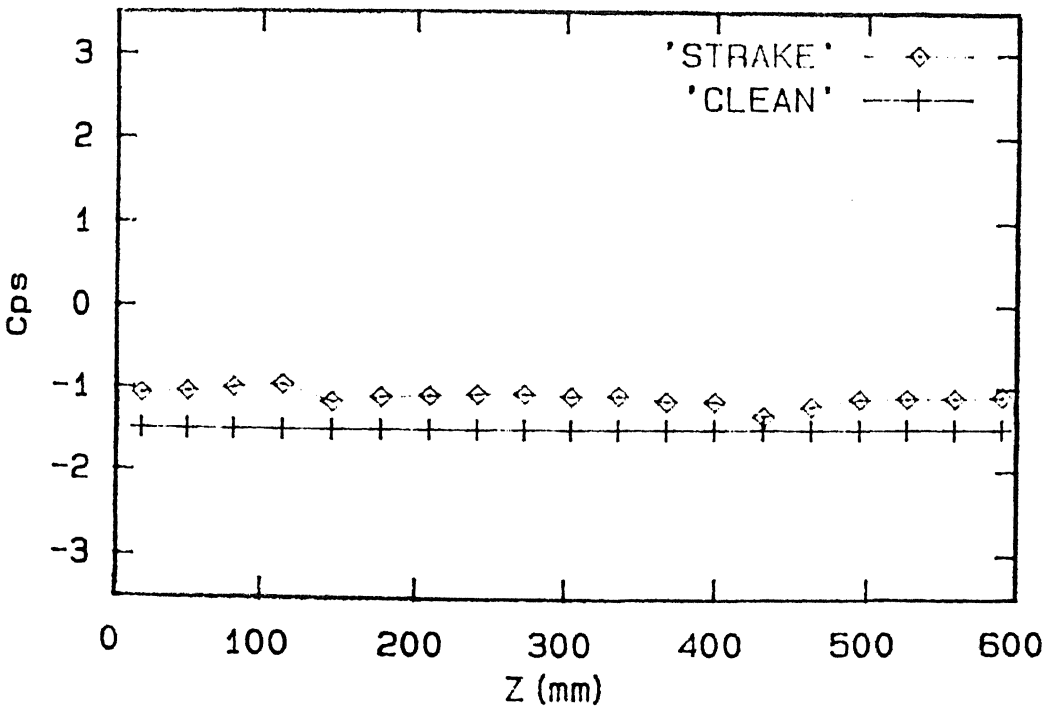

Spanwise Pressure Distribution

Figure 3.15: Pressure Distribution for $\alpha_{sp} = -150^o$ and $U_\infty = 9.0$ m/s

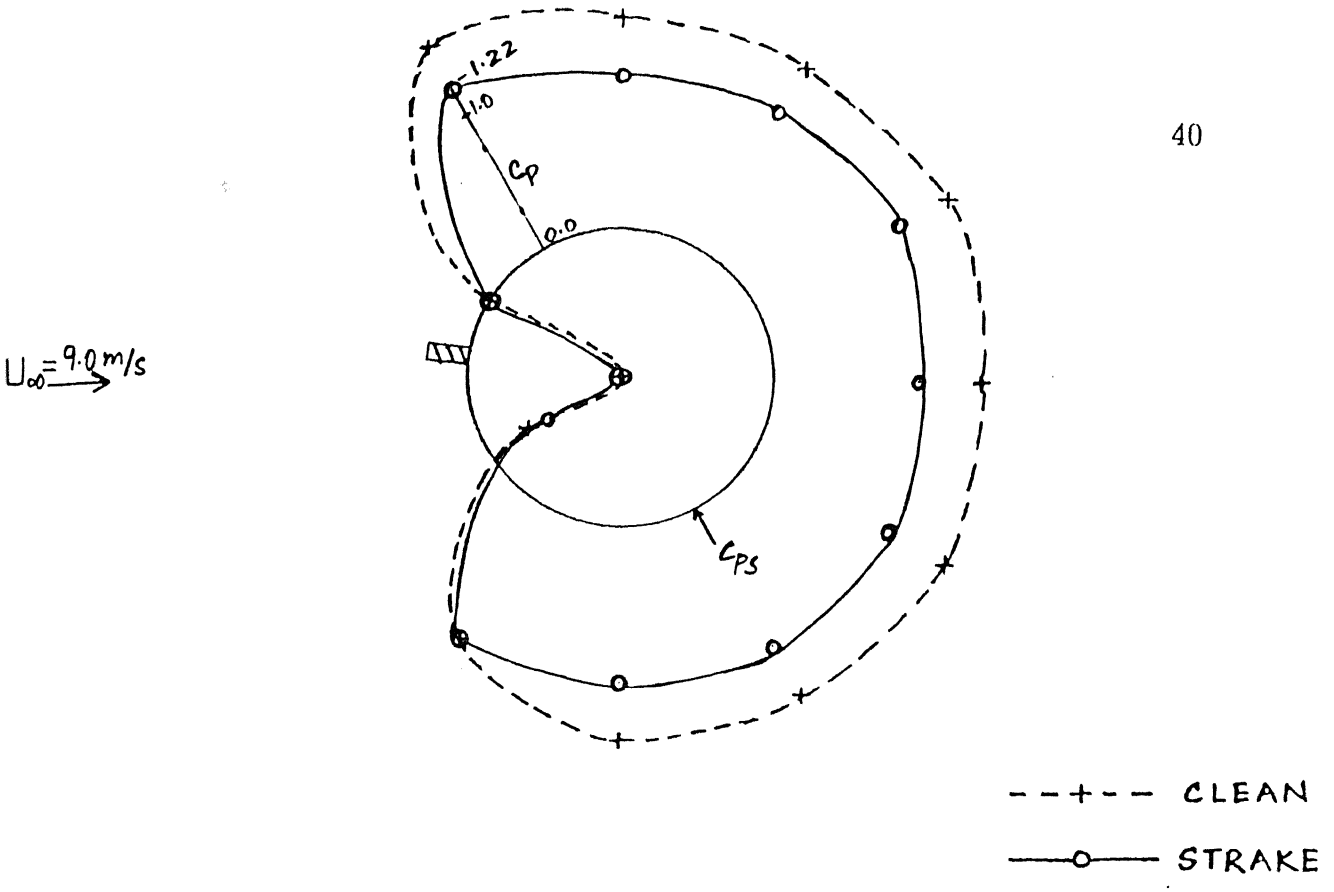

Radial Pressure Distribution

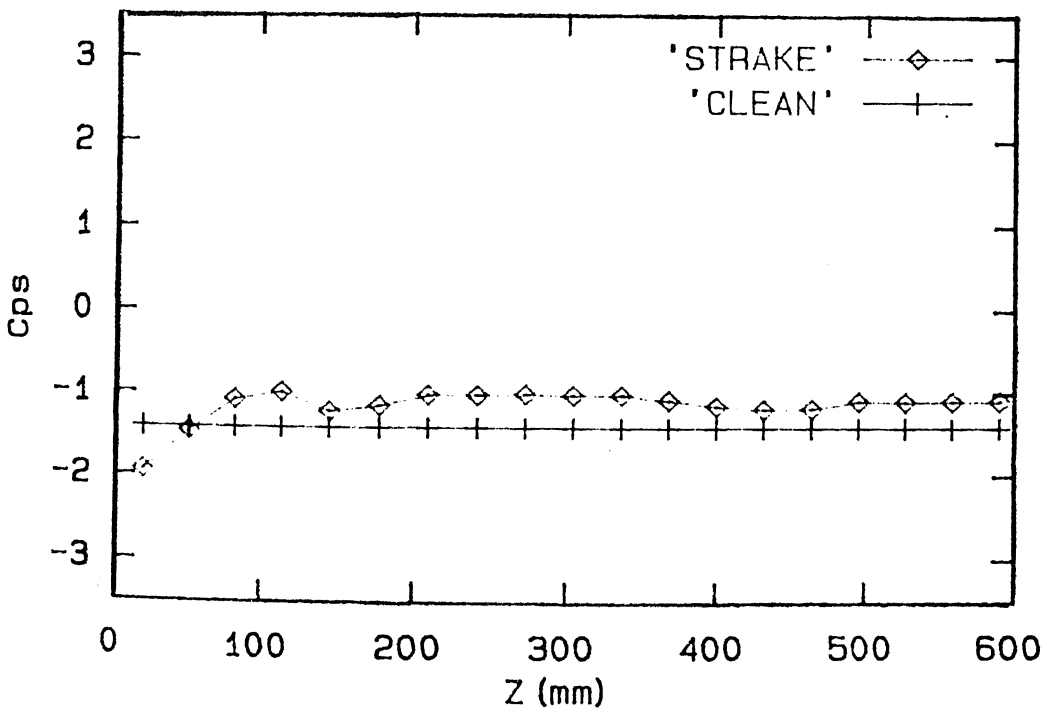

Spanwise Pressure Distribution

Figure 3.16: Pressure Distribution for $\alpha_{sp} = -120^{\circ}$ and $U_\infty = 9.0$ m/s

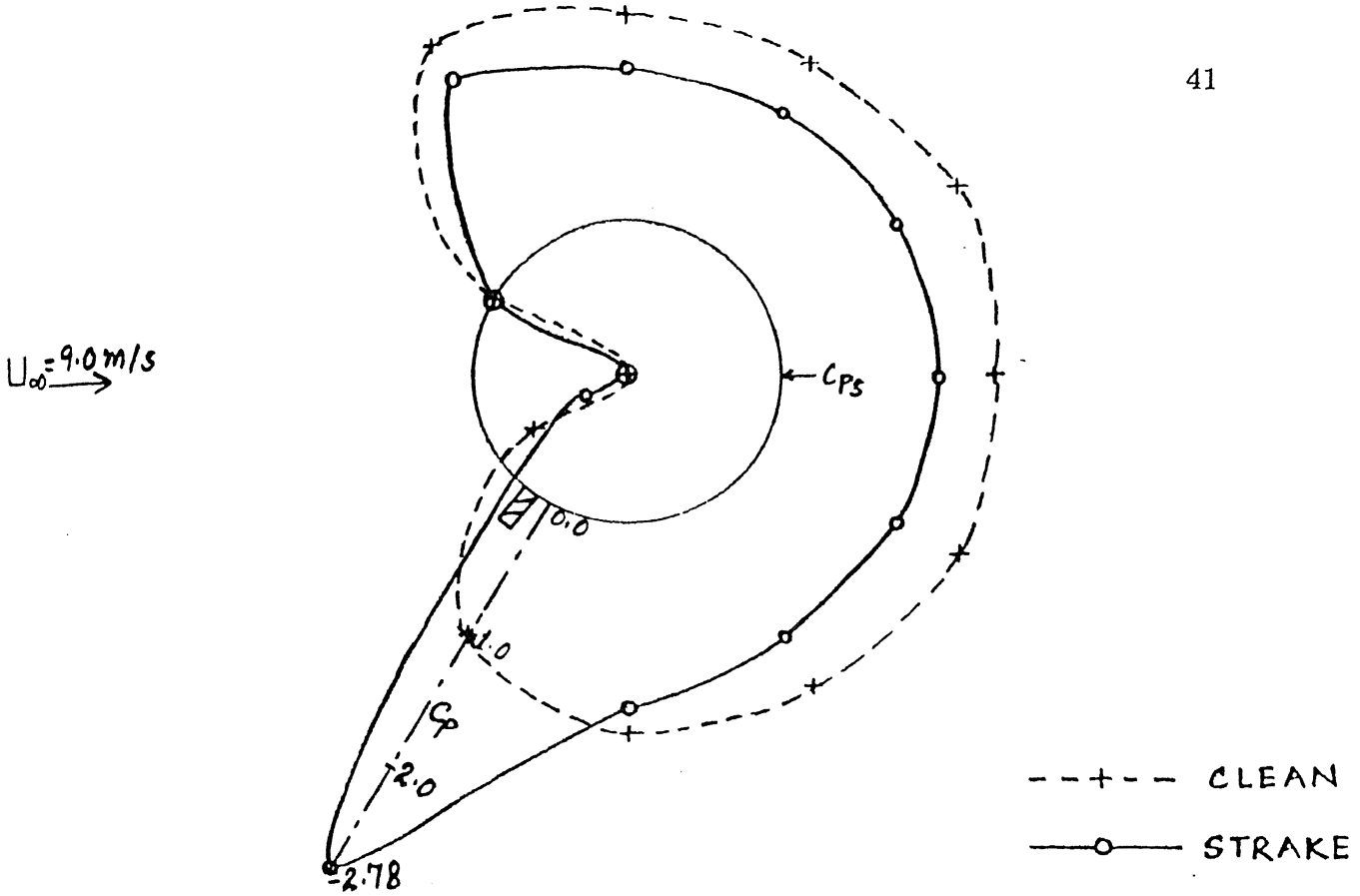

Radial Pressure Distribution

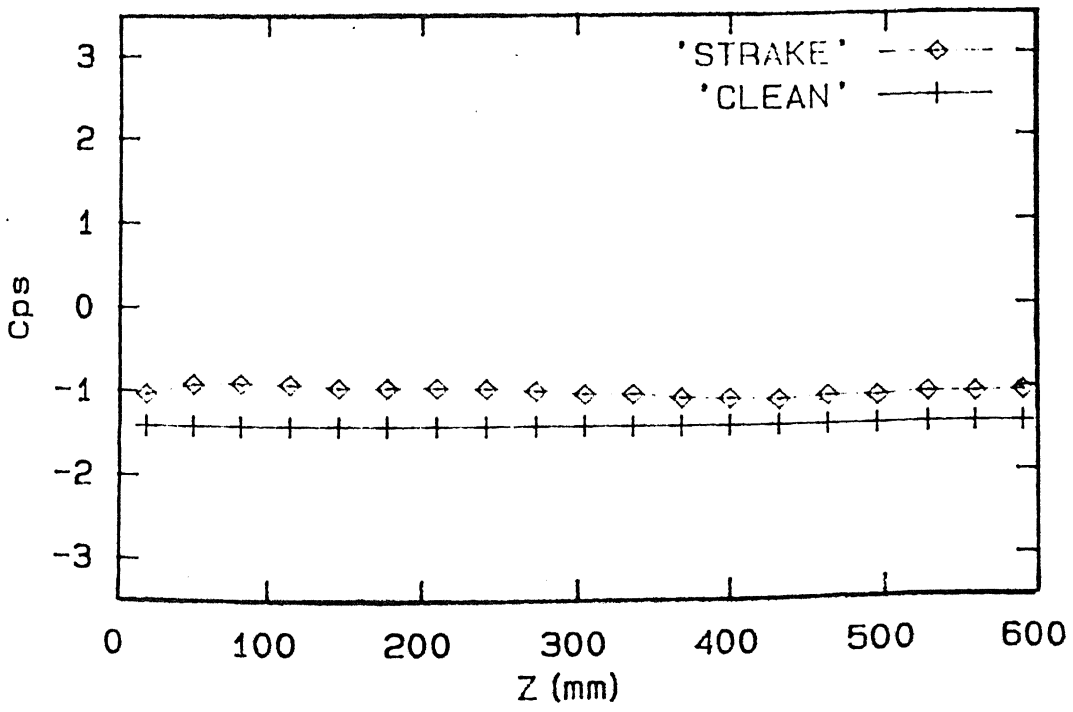

Spanwise Pressure Distribution

Figure 3.17: Pressure Distribution for $\alpha_{sp} = 180^o$ and $U_\infty = 9.0$ m/s

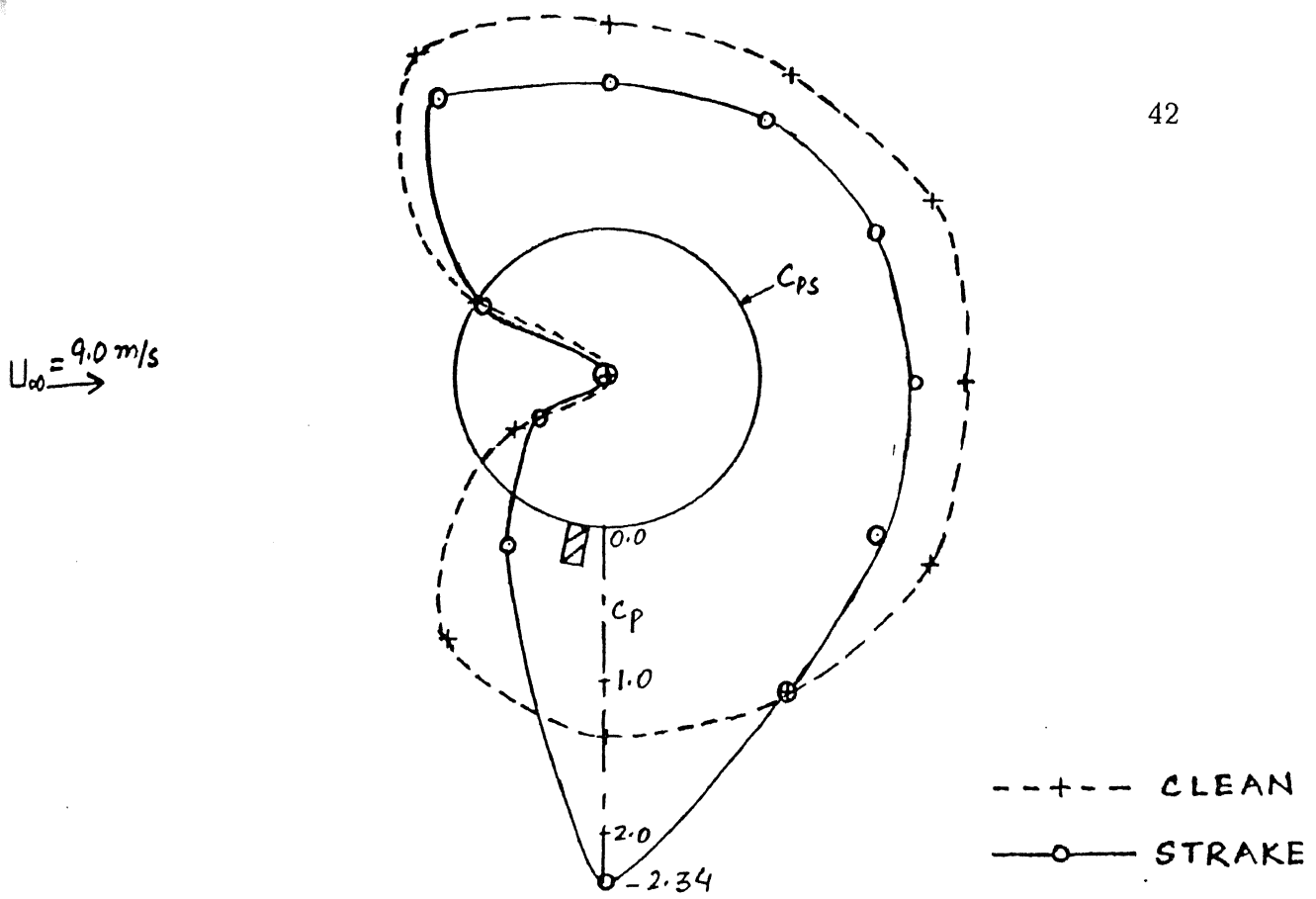

Radial Pressure Distribution

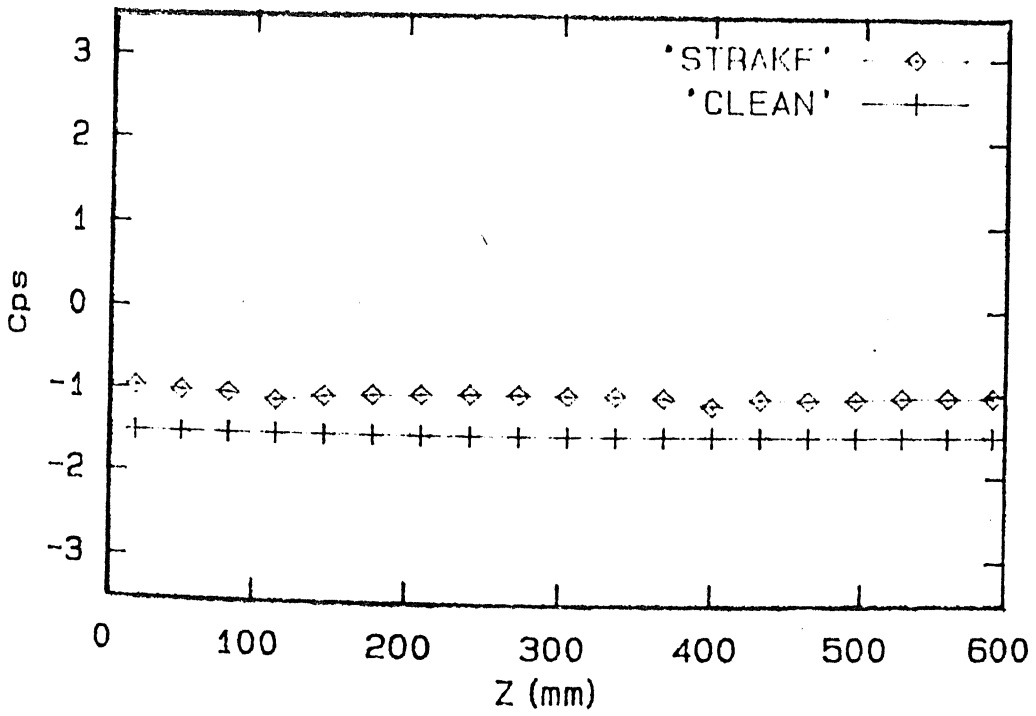

Spanwise Pressure Distribution

Figure 3.18: Pressure Distribution for $\alpha_{sp} = 150^o$ and $U_\infty = 9.0$ m/s

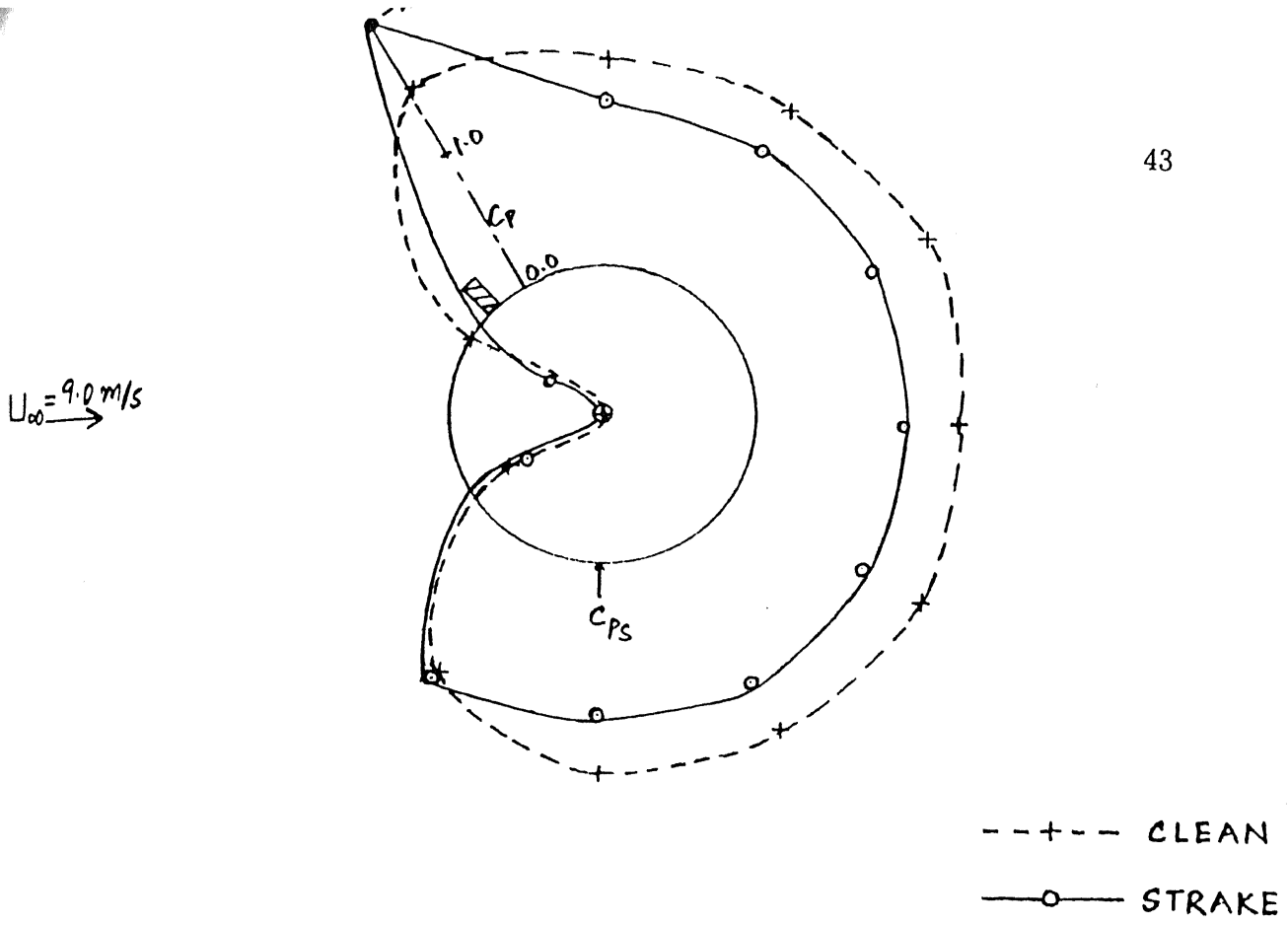

Radial Pressure Distribution

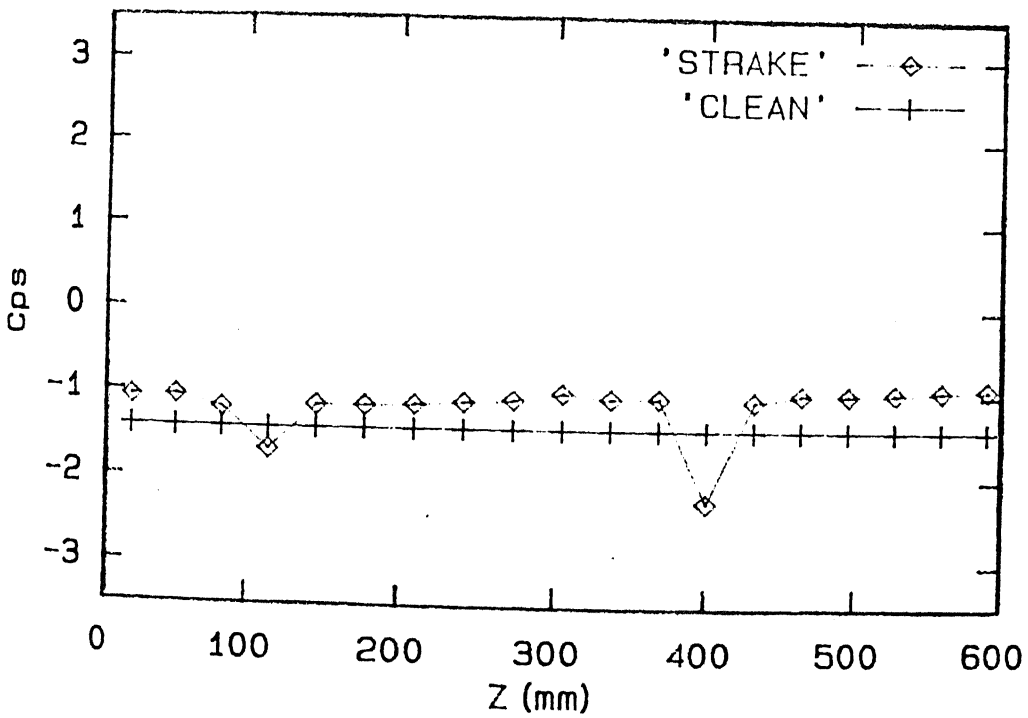

Spanwise Pressure Distribution

Figure 3.19: Pressure Distribution for $\alpha_{sp} = -90°$ and $U_\infty = 9.0$ m/s

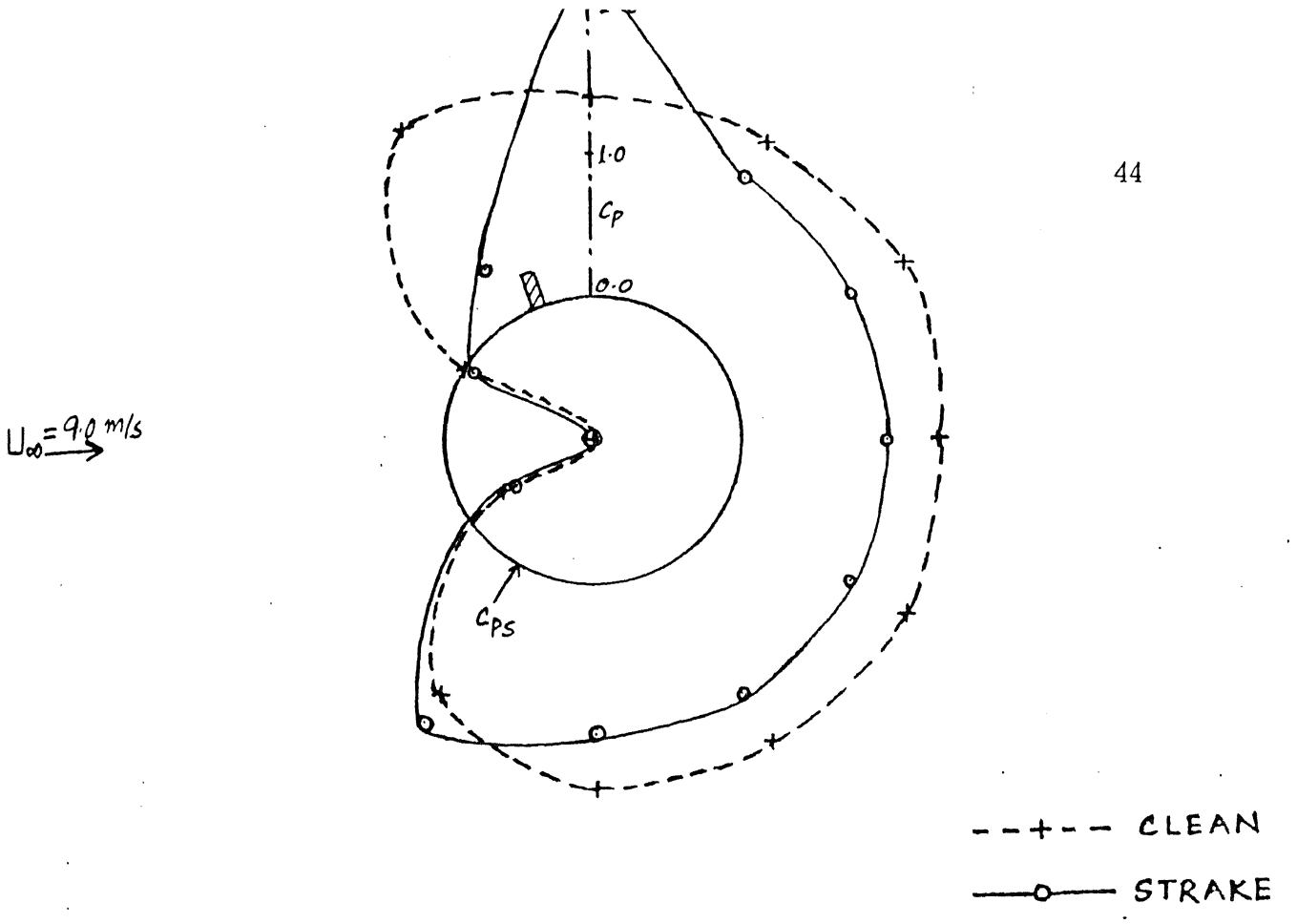

Radial Pressure Distribution

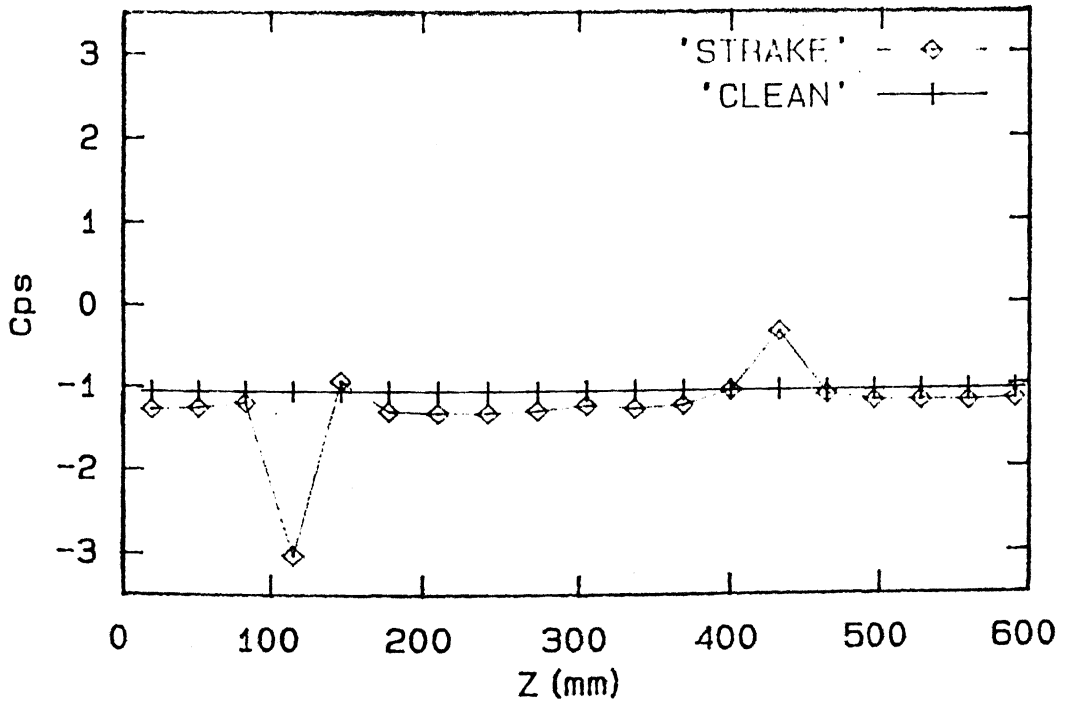

Spanwise Pressure Distribution

Figure 3.20: Pressure Distribution for $\alpha_{sp} = -60^o$ and $U_\infty = 9.0$ m/s

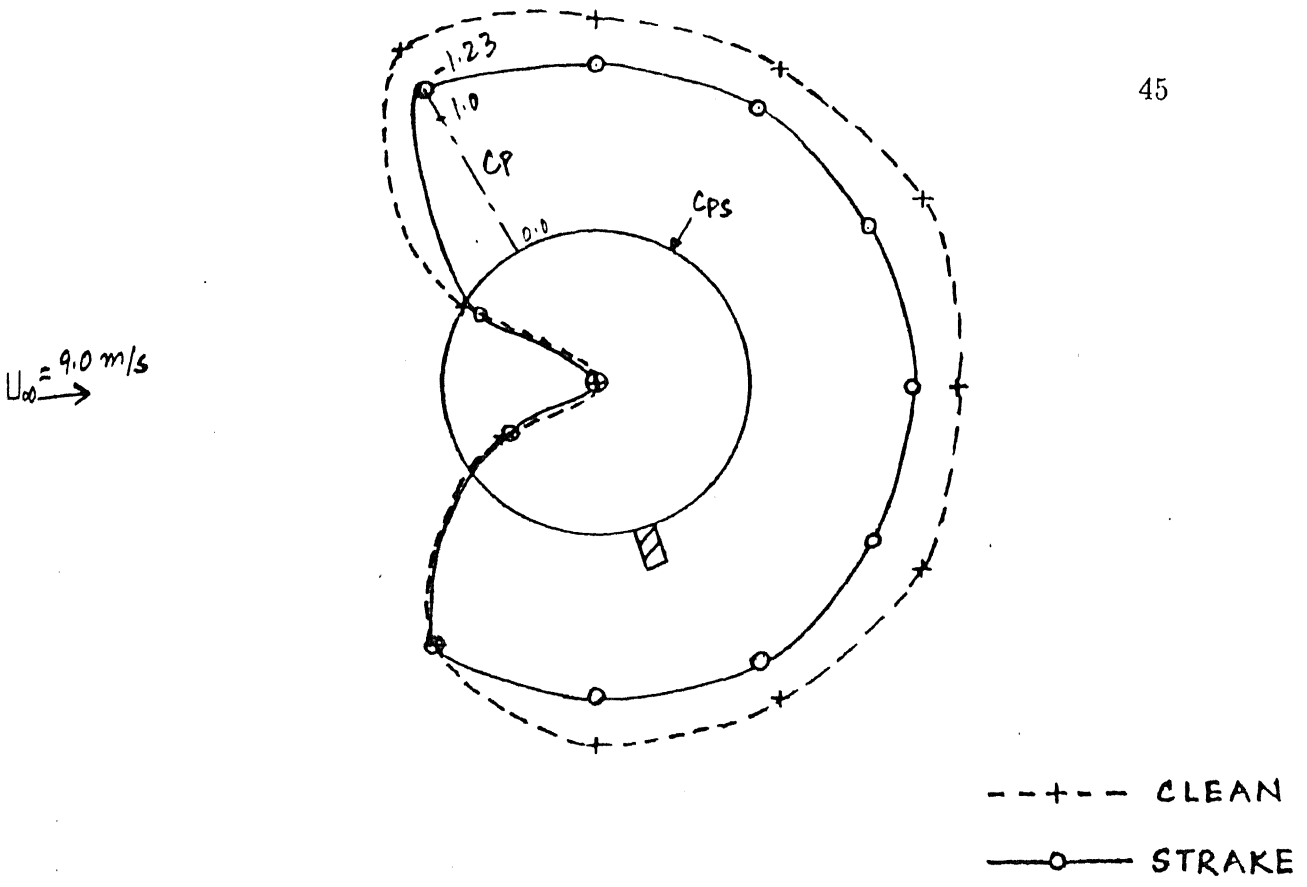

Radial Pressure Distribution

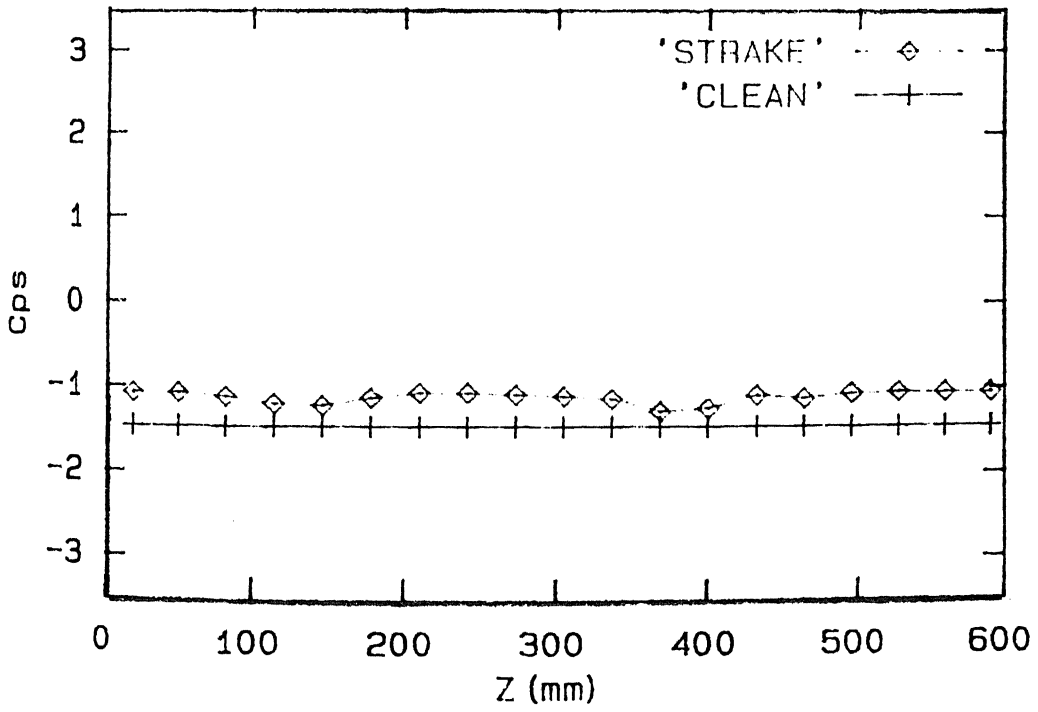

Spanwise Pressure Distribution

Figure 3.21: Pressure Distribution for $\alpha_{sp} = 120°$ and $U_\infty = 9.0$ m/s

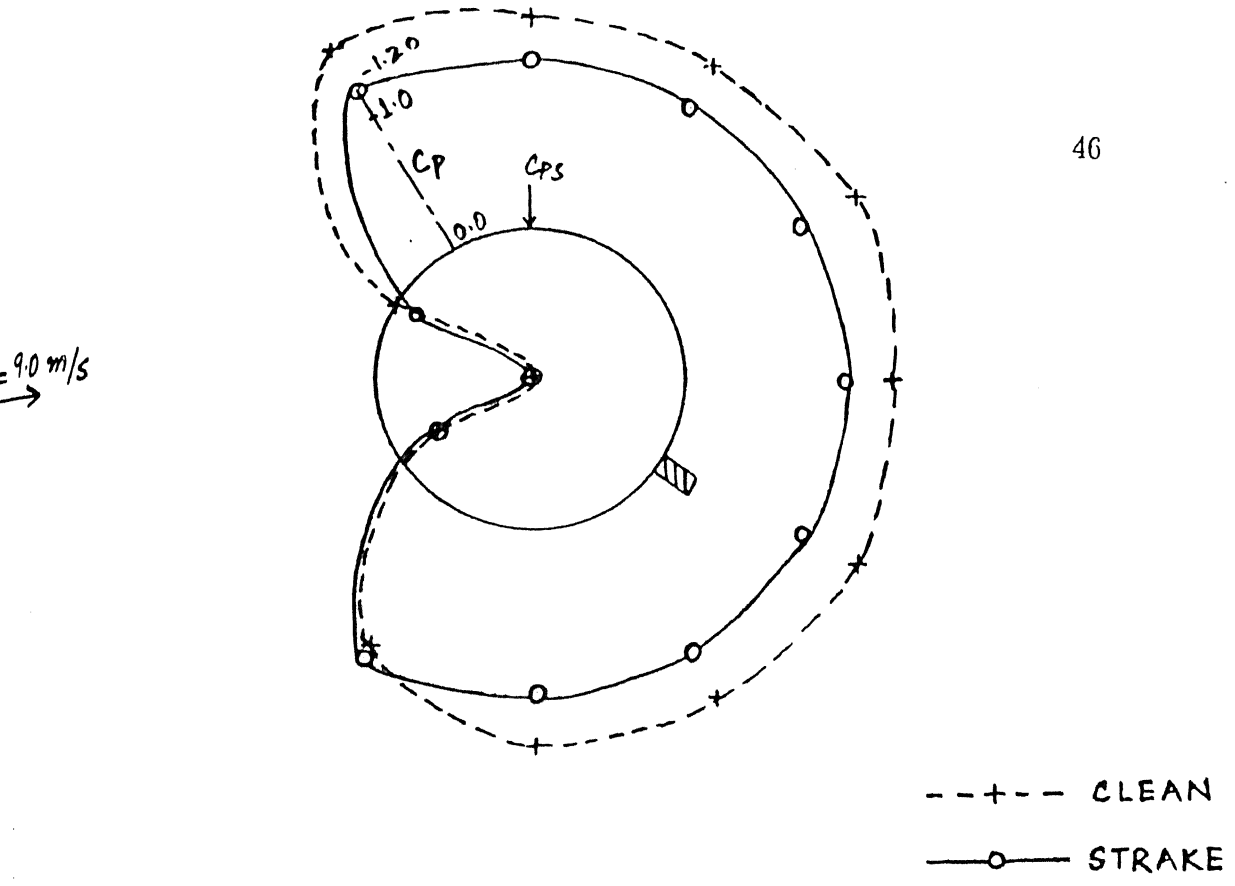

Radial Pressure Distribution

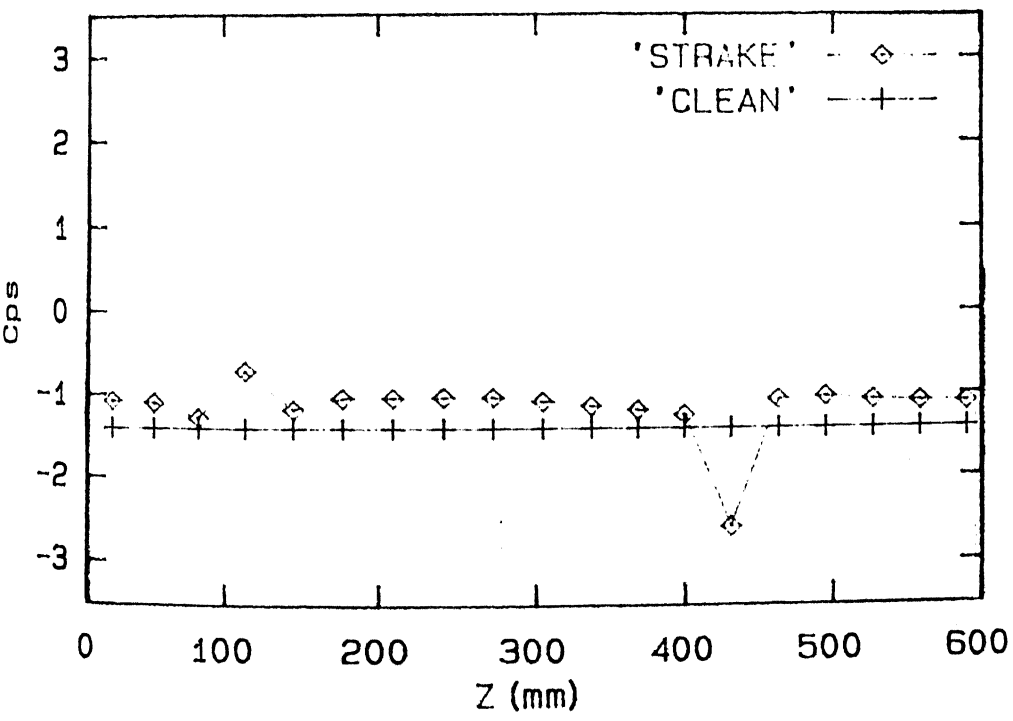

Spanwise Pressure Distribution

Figure 3.22: Pressure Distribution for $\alpha_{sp} = 90^{\circ}$ and $U_{\infty} = 9.0$ m/s

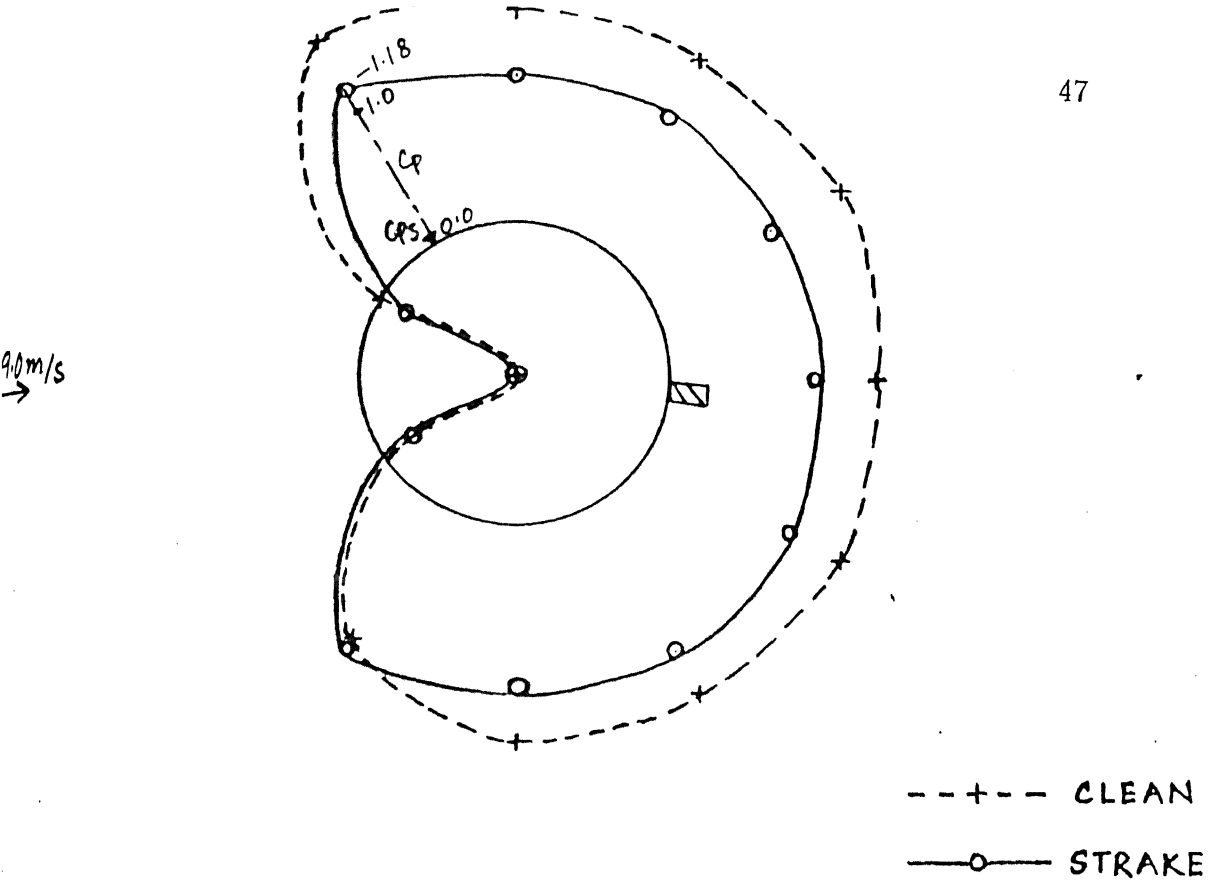

Radial Pressure Distribution

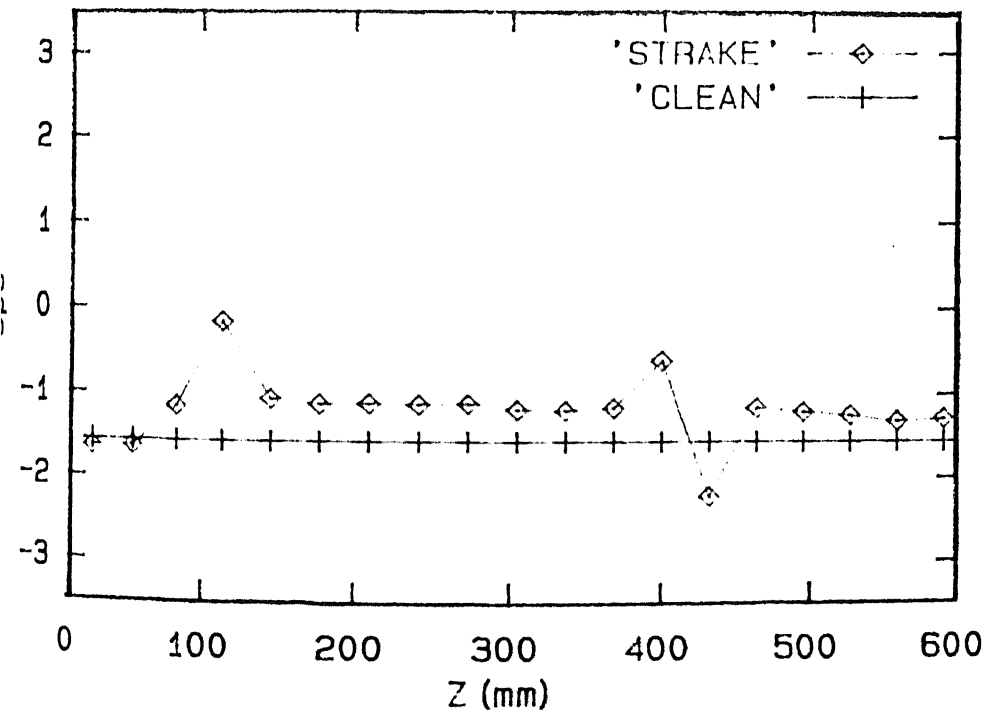

Spanwise Pressure Distribution

Figure 3.23: Pressure Distribution for $\alpha_{sp} = 60°$ and $U_\infty = 9.0$ m/s

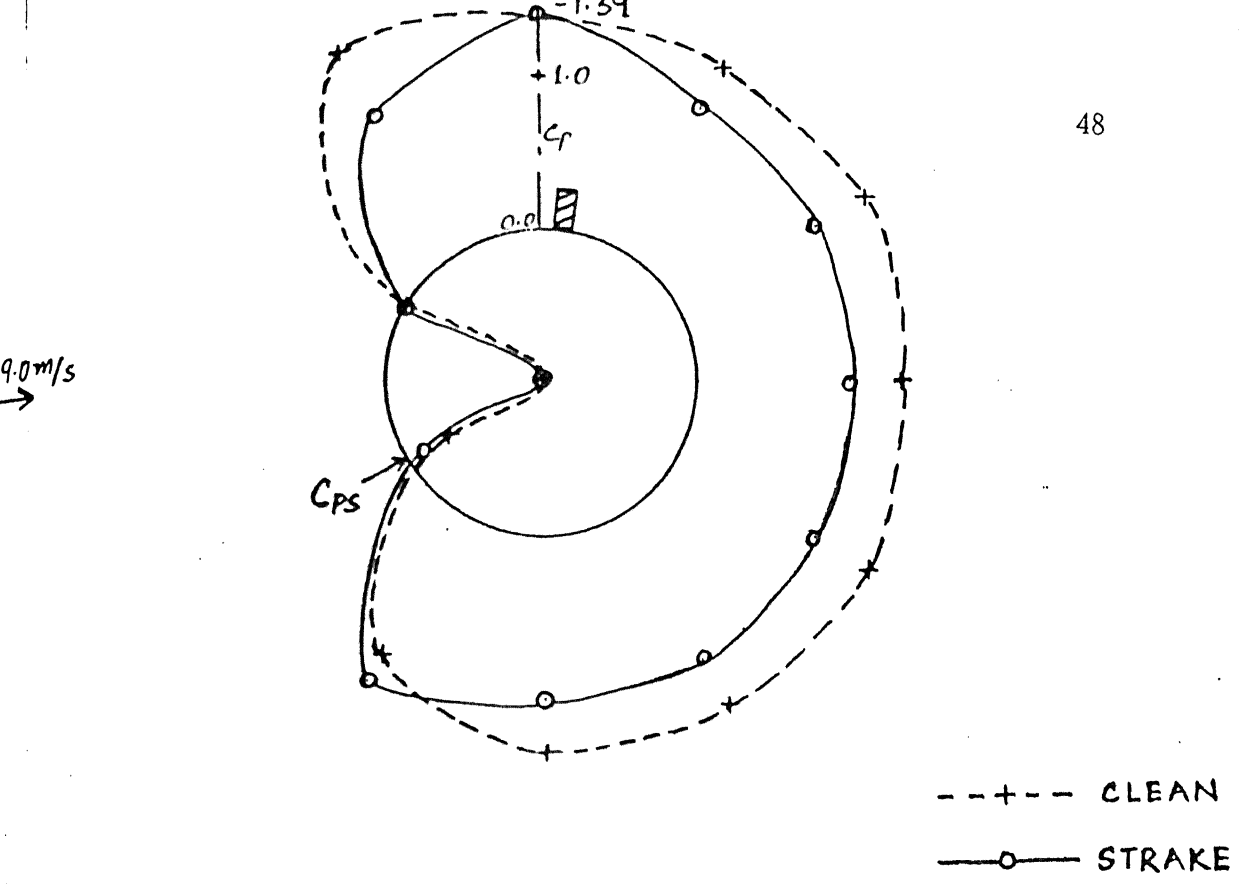

Radial Pressure Distribution

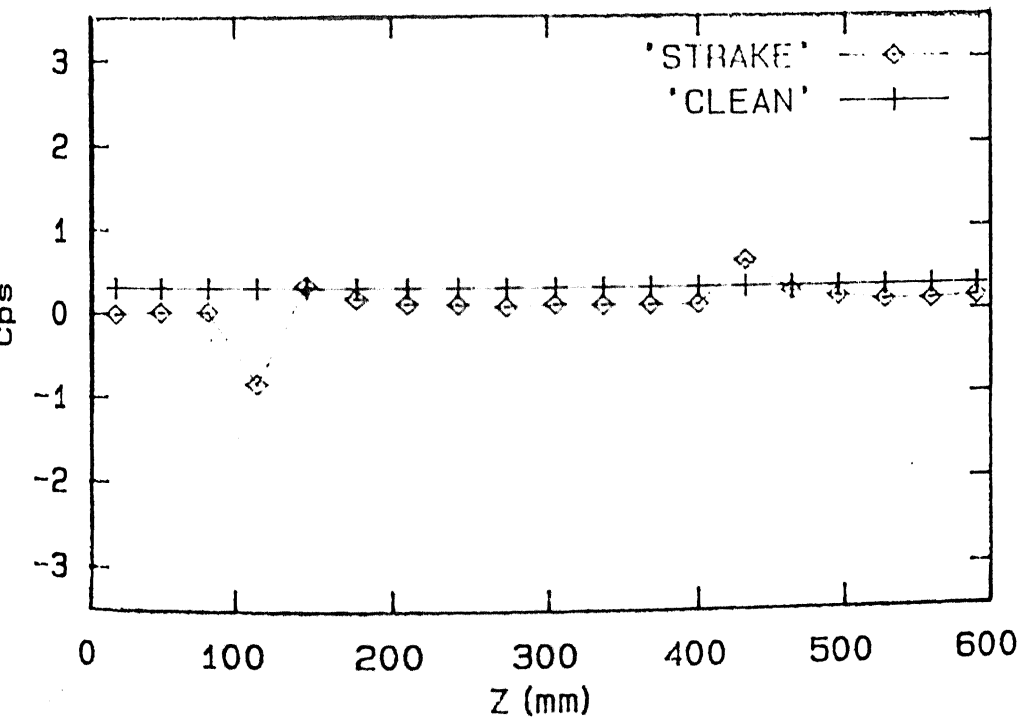

Spanwise Pressure Distribution

Figure 3.24: Pressure Distribution for $\alpha_{sp} = -30°$ and $U_\infty = 9.0$ m/s

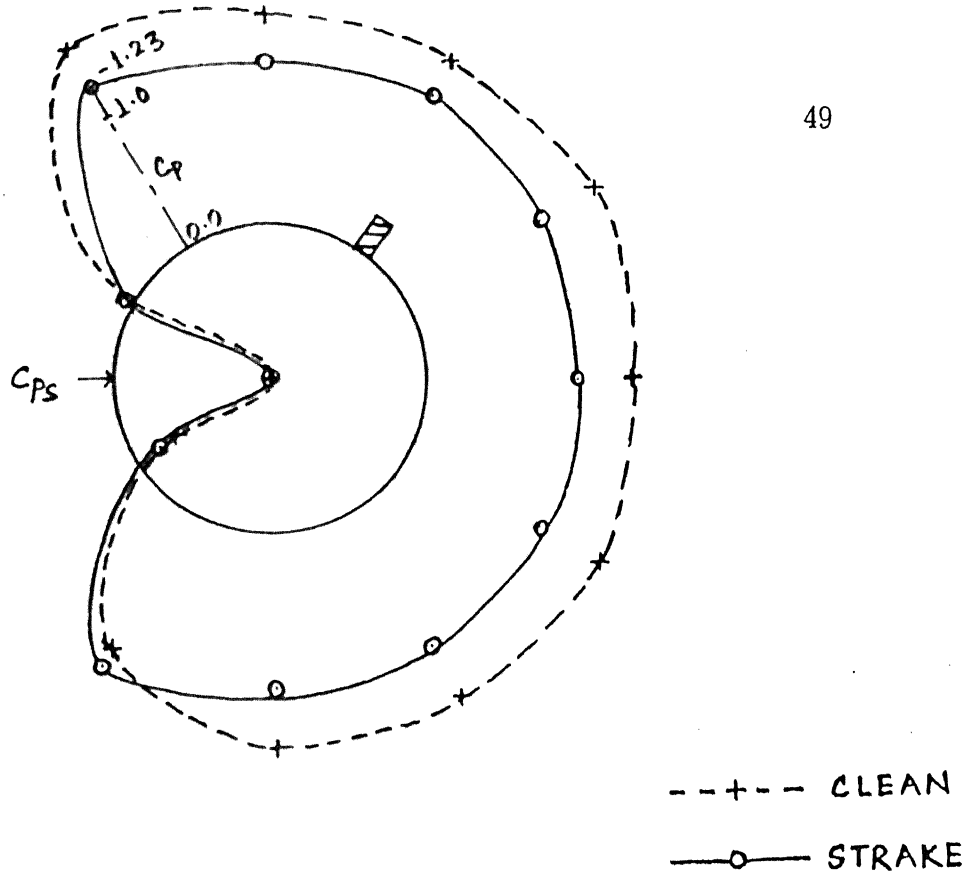

Radial Pressure Distribution

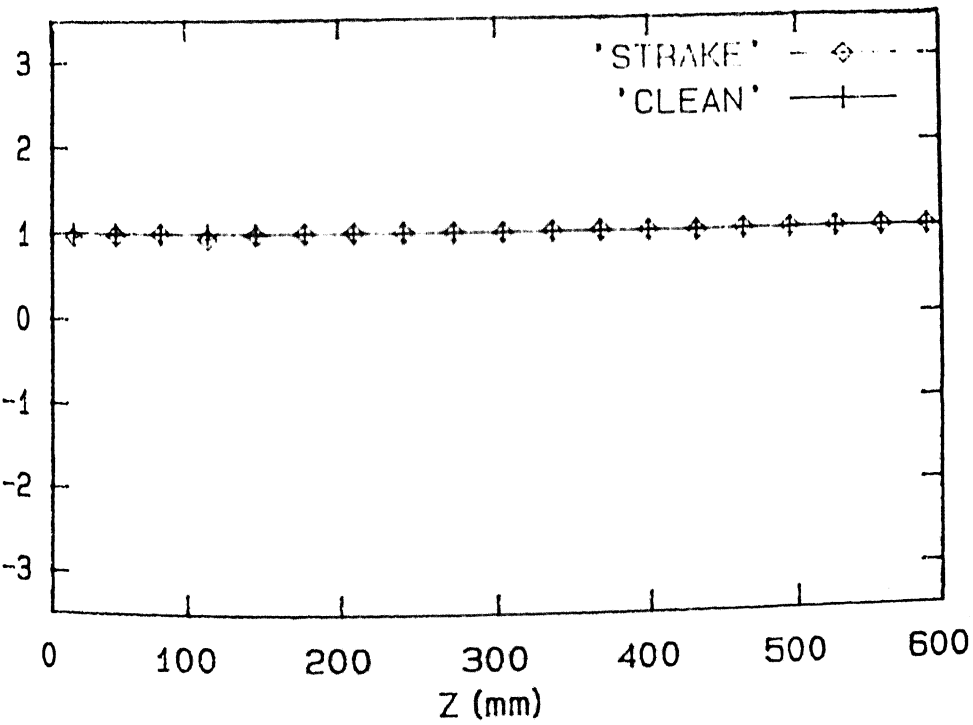

Spanwise Pressure Distribution

Figure 3.25: Pressure Distribution for $\alpha_{sp} = 0^o$ and $U_\infty = 9.0$ m/s

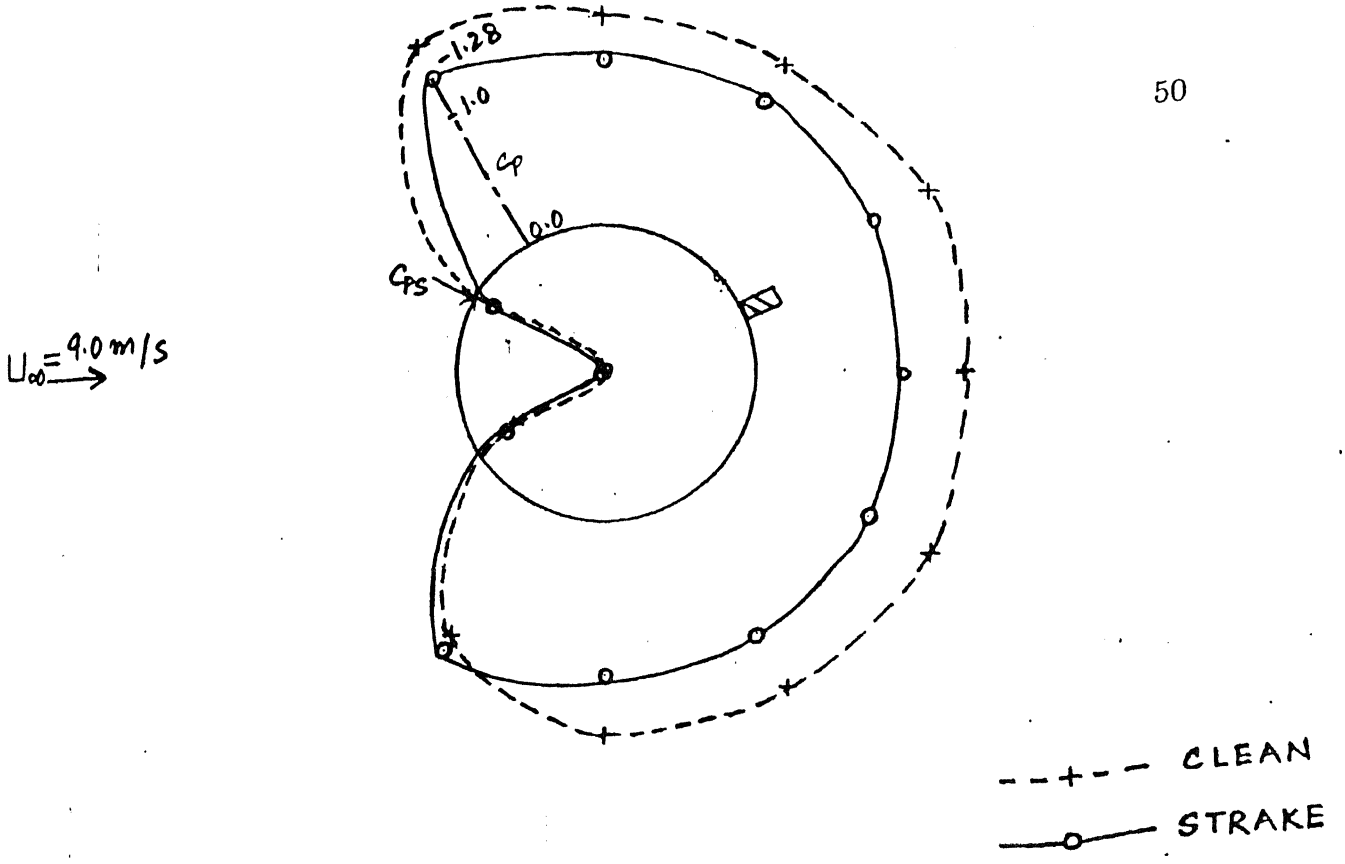

Radial Pressure Distribution

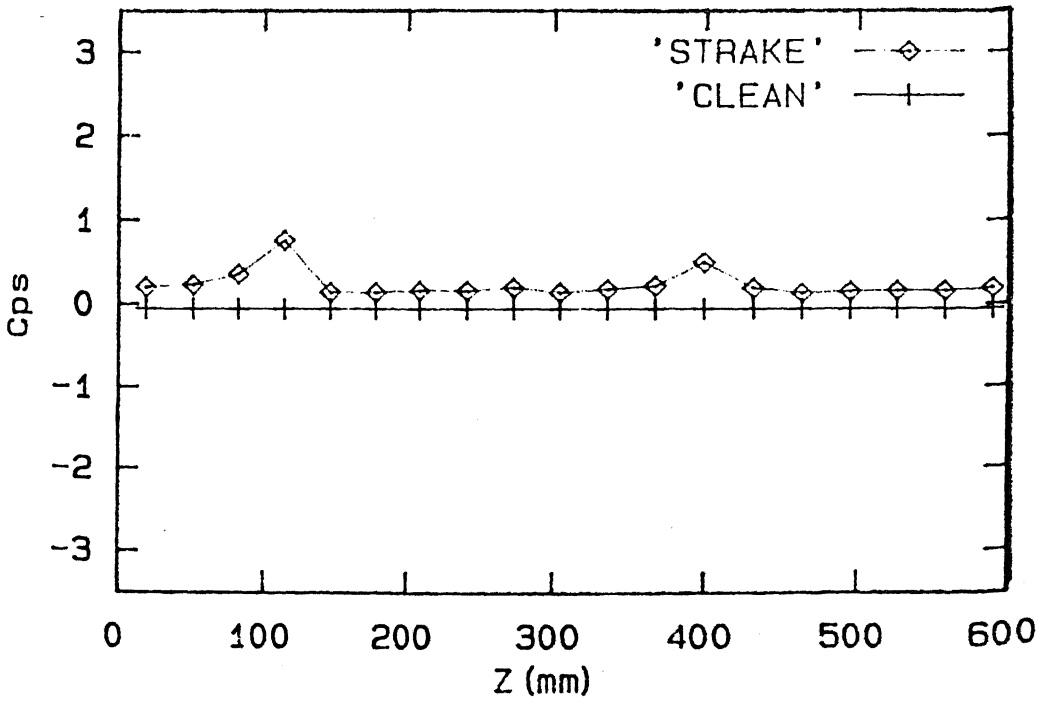

Spanwise Pressure Distribution

Figure 3.26: Pressure Distribution for $\alpha_{sp} = 30^o$ and $U_\infty = 9.0$ m/s

Chapter 4

CONCLUSION AND SUGGESTIONS FOR FUTURE WORK

4.1 Conclusion

The aim of the present work was to see the effect of helical strake on the pressure distributions of a circular cylinder. In the present work, a single start pattern of helical strake was used on the circular cylinder to investigate the pressure distributions.

The pressure distributions show different trends depending upon the location of strake. The only effect which is independent of the location of strake is the slight increase in pressure in the midriff and rear regions of the cylinder which is seen for all the flow configurations. The general effect of the helical strake is that it introduces a strong asymmetry in the pressure distributions both along the span as well as upward and downward/forward and backward at each span. This is caused

by the introduction of three dimensionality in the mean flow field because of the presence of helical strake. This three dimensionality may also cause breaking up of fluctuating flow field which is responsible for the periodic vortex shedding and hence the flow induced oscillations of a circular cylinder. This breaking up of fluctuating flow field caused by the strong three dimensionality of the mean flow field is likely to be responsible for the reduction in flow induced oscillations of a circular cylinder.

4.2 Suggestions for Future Work

The following possibilities are realized at this stage for future work in this field of study:

- In the present work, the effect of helical strake has been investigated only on the mean flow field. A separate study is required to see the effect of strakes on the fluctuating flow field of a circular cylinder. The investigation of fluctuating flow field will give a better picture of the reduction of flow induced oscillations.
- The effect of single start pattern of strake has been investigated, which doesn't cover the whole of the cylinder. So, cylinders with double or triple start pattern of helical strake may be investigated in a separate study.
- A flow visualization experiment may be performed in a smoke tunnel to visualize the effect of helical strake on a circular cylinder

Appendix A

COEFFICIENT OF PRESSURE VALUES

The coefficient of pressure values for straked cylinder are given in this appendix. The values for radial and spanwise distributions at two speeds are given in four tables. These values were calculated from the experimental data using the formula:

$$C_p = \frac{P - P_\infty}{\frac{1}{2}\rho {U_\infty}^2} \tag{A.1}$$

Table A.1: C_p values for radial distribution at mid-span for $U_\infty = 4.5$ m/s

α_{hs}(deg) / α_{sp}(deg)	-180	-150	-120	-90	-60	-30	0	30	60	90	120	150
0	1.00	1.00	1.00	1.00	1.00	1.00	1.00	1.00	1.00	1.00	1.00	1.00
30	0.19	0.16	0.07	0.08	0.00	-0.09	0.09	0.57	0.13	-0.04	-0.08	0.18
60	-1.18	-1.15	-1.19	-1.24	-1.26	-1.26	-1.25	-1.92	-0.38	-0.98	-1.14	-1.18
90	-0.93	-1.03	-1.06	-1.00	-1.03	-1.03	-1.03	-1.01	-2.04	-1.18	-0.97	-0.90
120	-0.95	-1.05	-1.09	-1.06	-0.93	-1.07	-1.05	-1.04	-1.17	-1.14	-1.03	-0.96
150	-0.97	-1.05	-1.09	-1.08	-1.06	-0.92	-1.12	-1.07	-1.08	-1.11	-1.07	-0.95
180	-1.00	-1.06	-1.08	-1.06	-1.02	-1.03	-0.98	-0.98	-1.06	-1.05	-1.02	-0.90
-150	-0.97	-1.08	-1.17	-1.08	-1.05	-1.07	-1.12	-0.98	-1.10	-1.03	-1.00	-0.92
-120	-0.94	-0.99	-1.19	-1.34	-1.03	-1.04	-1.11	-1.04	-0.97	-1.04	-1.02	-0.92
-90	-0.90	-1.00	-1.00	-1.86	-1.22	-1.01	-1.09	-1.04	-1.06	-0.93	-1.00	-0.90
-60	-1.00	-0.99	-0.94	-0.29	-2.60	-0.89	-1.03	-1.12	-1.28	-1.18	-1.00	-1.05
-30	0.25	0.36	0.40	0.45	0.69	0.16	0.44	0.42	0.39	0.13	0.20	0.30

Table A.2: C_p values for radial distribution at mid-span for $U_\infty = 9.0$ m/s

α_{hs}(deg) / α_{sp}(deg)	-180	-150	-120	-90	-60	-30	0	30	60	90	120	150
0	1.00	1.00	1.00	1.00	1.00	1.00	1.00	1.00	1.00	1.00	1.00	1.00
30	0.18	0.13	0.10	0.05	0.03	-0.12	0.07	0.58	0.10	-0.10	-0.11	0.14
60	-1.18	-1.20	-1.23	-1.18	-1.26	-1.30	-1.22	-2.05	-0.42	-1.07	-1.23	-1.28
90	-0.96	-1.08	-1.07	-0.99	-1.02	-1.05	-1.00	-1.09	-2.14	-1.39	-1.03	-1.09
120	-0.97	-1.09	-1.08	-1.03	-1.00	-1.05	-1.03	-1.07	-1.12	-1.13	-1.16	-1.13
150	-0.96	-1.07	-1.09	-1.03	-1.03	-1.04	-1.02	-1.07	-1.04	-1.10	-1.05	-1.06
180	-0.97	-1.09	-1.10	-1.05	-1.04	-1.05	-0.96	-1.03	-1.03	-1.07	-1.02	-0.97
-150	-1.10	-1.06	-1.11	-1.08	-1.04	-1.09	-1.03	-1.02	-1.02	-1.06	-1.03	-0.99
-120	-1.09	-1.05	-1.11	-1.39	-1.03	-1.06	-1.02	-1.04	-1.02	-1.06	-1.03	-1.01
-90	-1.03	-1.05	-1.04	-2.34	-1.22	-1.02	-0.99	-0.99	-1.03	-1.03	-1.03	-0.99
-60	-1.10	-1.10	-1.02	-0.28	-2.78	-0.92	-1.03	-1.13	-1.24	-1.21	-1.15	-1.16
-30	0.22	0.29	0.34	0.45	0.68	0.14	0.42	0.43	0.36	0.10	0.18	0.24

Table A.3: C_p values for spanwise distribution for $U_\infty = 4.5$ m/s

α_{hs}(deg) Z(mm)	-180	-150	-120	-90	-60	-30	0	30	60	90	120	150
19.0	-1.30	-0.97	-1.08	-1.00	-0.86	-1.10	-1.13	-1.01	-1.28	0.00	1.00	0.24
50.8	-1.30	-0.98	-1.08	-1.01	-0.83	-1.03	-1.14	-1.01	-1.34	0.09	1.03	0.26
82.5	-1.01	-0.98	-1.10	-1.06	-0.93	-0.93	-1.34	-1.09	-1.29	0.09	1.03	0.37
114.3	-0.09	-0.65	-1.21	-1.03	-0.93	-0.93	-1.04	-1.80	-2.78	-0.87	0.91	0.75
146.0	-1.07	-1.19	-1.21	-1.12	-1.05	-1.14	-1.09	-0.98	-0.85	0.37	1.02	0.13
177.8	-1.17	-0.98	-1.16	-1.10	-1.06	-1.07	-1.16	-1.04	-1.21	0.20	1.03	0.13
209.5	-1.16	-0.96	-1.10	-1.09	-0.99	-1.07	-1.12	-1.03	-1.23	0.16	1.03	0.16
241.3	-1.14	-0.96	-1.08	-1.07	-1.02	-1.05	-1.04	-1.00	-1.23	0.14	1.02	0.17
273.0	-1.15	-0.95	-1.08	-1.05	-1.01	-1.07	-1.06	-1.00	-1.25	0.11	1.00	0.21
304.8	-1.18	-1.03	-1.09	-1.08	-1.02	-1.07	-1.11	-1.04	-1.28	0.13	1.00	0.18
336.5	-1.18	-1.02	-1.12	-1.06	-1.11	-1.09	-1.08	-1.00	-1.25	0.11	1.02	0.20
368.3	-1.10	-1.08	-1.27	-1.07	-1.06	-1.09	-1.12	-0.96	-1.28	0.11	1.02	0.26
400.0	-0.52	-1.08	-1.21	-1.25	-1.03	-1.09	-1.19	-2.09	-1.06	0.11	1.02	0.51
431.8	-2.27	-2.08	-1.12	-1.10	-1.14	-1.26	-1.10	-0.98	-0.23	0.65	1.01	0.21
463.5	-1.16	-0.95	-1.16	-1.10	-1.15	-1.14	-1.30	-0.95	-1.14	0.29	1.03	0.15
495.3	-1.16	-0.94	-1.14	-1.11	-1.14	-1.09	-1.10	-0.95	-1.16	0.21	1.03	0.18
527.0	-1.17	-0.94	-1.13	-1.11	-1.16	-1.10	-1.12	-0.95	-1.23	0.14	1.03	0.21
558.8	-1.24	-0.96	-1.15	-1.10	-1.14	-1.10	-1.15	-0.95	-1.25	0.14	1.02	0.20
590.5	-1.18	-0.98	-1.17	-1.10	-1.16	-1.10	-1.13	-0.91	-1.23	0.15	1.02	0.23

Table A.4: C_p values for spanwise distribution for $U_\infty = 9.0$ m/s

α_{hs}(deg) Z(mm)	-180	-150	-120	-90	-60	-30	0	30	60	90	120	150
19.0	-1.64	-1.08	-1.05	-0.98	-1.04	-1.07	-1.94	-1.08	-1.28	-0.02	0.96	0.20
50.8	-1.63	-1.10	-1.05	-1.02	-0.92	-1.04	-1.46	-1.06	-1.26	0.01	0.98	0.23
82.5	-1.15	-1.28	-1.09	-1.04	-0.91	-0.99	-1.08	-1.20	-1.20	0.02	1.00	0.36
114.3	-0.15	-0.71	-1.17	-1.12	-0.92	-0.95	-0.99	-1.68	-3.03	-0.85	0.94	0.76
146.0	-1.06	-1.18	-1.19	-1.06	-0.96	-1.16	-1.22	-1.15	-0.94	0.33	0.98	0.14
177.8	-1.12	-1.04	-1.10	-1.04	-0.96	-1.10	-1.15	-1.15	-1.31	0.17	1.00	0.14
209.5	-1.11	-1.03	-1.04	-1.03	-0.96	-1.08	-1.02	-1.13	-1.33	0.11	1.01	0.16
241.3	-1.12	-1.03	-1.04	-1.02	-0.97	-1.06	-1.02	-1.10	-1.33	0.10	1.01	0.16
273.0	-1.11	-1.03	-1.06	-1.02	-1.00	-1.06	-1.01	-1.07	-1.30	0.07	1.01	0.20
304.8	-1.18	-1.08	-1.08	-1.03	-1.04	-1.09	-1.02	-0.99	-1.24	0.10	1.00	0.14
336.5	-1.19	-1.14	-1.11	-1.03	-1.04	-1.08	-1.02	-1.05	-1.28	0.09	1.01	0.18
368.3	-1.16	-1.19	-1.26	-1.05	-1.09	-1.15	-1.08	-1.04	-1.24	0.09	1.01	0.22
400.0	-0.60	-1.25	-1.22	-1.15	-1.10	-1.15	-1.15	-2.26	-1.06	0.09	1.00	0.50
431.8	-2.22	-2.60	-1.07	-1.06	-1.12	-1.33	-1.19	-1.07	-0.35	0.61	0.99	0.19
463.5	-1.16	-1.07	-1.11	-1.07	-1.08	-1.21	-1.18	-0.99	-1.12	0.24	1.01	0.13
495.3	-1.21	-1.03	-1.05	-1.06	-1.09	-1.12	-1.09	-0.99	-1.20	0.17	1.01	0.15
527.0	-1.25	-1.08	-1.03	-1.04	-1.06	-1.11	-1.10	-0.97	-1.20	0.12	1.01	0.16
558.8	-1.32	-1.10	-1.04	-1.04	-1.07	-1.11	-1.09	-0.94	-1.21	0.12	1.01	0.16
590.5	-1.29	-1.11	-1.04	-1.04	-1.05	-1.10	-1.09	-0.92	-1.19	0.15	1.00	0.19

Table For a Fixed Configuration The Values of Z w.r.t. α_{hs}

α_{hs}(deg)	Z(mm)
7.3	0.0
30.0	19.6
60.0	45.5
90.0	71.4
120.0	97.4
150.0	123.3
180.0	149.2
-150.0	175.1
-120.0	201.1
-90.0	227.0
-60.0	252.9
-30.0	278.9
0.0	304.8
30.0	330.7
60.0	356.6
90.0	382.6
120.0	408.5
150.0	434.4
180.0	460.4
-150.0	486.3
-120.0	512.2
-90.0	538.2
-60.0	564.1
-30.0	590.0
-7.3	609.6

References

[1] C. Scruton and A. R. Flint, Wind-excited oscillations of structures, Proc. Inst. Civ. Eng., 27(1964) 673-702.

[2] M. V. Morkovin, Flow around a circular cylinder - a kaleidoscope of challenging fluid phenomena, Am. Soc. Mech. Eng. Symp. on Fully separated flow, 1964, pp. 102-118.

[3] C. Scruton and E. W. E. Rogers, Wind effects on buildings and other structures, Philos. Trans. R. Soc. London, Ser. A, 269(1971) 353-383.

[4] G. V. Parkinson, Mathematical models of flow-induced vibrations of bluff bodies, in E. Naudascher(Ed.), Flow Induced Structural Vibrations, Springer, Berlin, 1974, pp. 81-122.

[5] M. M. Zdravkovich, Review and Classification of various aerodynamic and hydrodynamic means for suppressing vortex shedding, J. Wind Eng. Ind. Aerodyn., 7(1981) 145- 189.

[6] C. Scruton and D. E. Walshe, A means of avoiding wind-excited oscillation of structures with circular or nearly circular cross section, Natl. Phys. Lab.(U.K.), Aero Rep. 335 (1957).

[7] L. Woodgate and J. F. M. Maybrey, Further experiments on the use of helical strakes for avoiding wind excited oscillations of stuctures of circular or nearly circular section, Natl. Phys. Lab.(U.K.), Aero Rep. 381 (1959).

[8] C. F. Cowdrey and J. A. Lawes, Drag Measurements at high Reynolds numbers of a circular cylinder fitted with three helical strakes, Natl. Phys. Lab.(U.K.), Aero Rep. 384 (1959).

[9] H. Ruscheweyh, Tip effect on the vortex excited oscillation of a model stack with and without efflux stream, Symp. on Flow Induced Structural Vibrations, Karlsruhe, W. Germany, 1972, Suppl., 101-103.

[10] B. J. Vickery and R. D. Watkins, Flow induced vibrations of cylindrical structures, in R. Silvester(Ed.), Proc. 1st Aust. Conf. on Hydraulics and Fluid Mechanics, Pergamon, 1964, pp. 213-241.

[11] I. S. Gartshore, J. Khanna and S. Laccinole, The effectiveness of vortex spoilers on a circular cylinder in smooth and turbulent flow, Proc. 5th Int. Conf. on Wind Engineering, Fort Collins, CO, 1978.

[12] H. Y. Wong and A. Kokkalis, A Comparative Study of Three Aerodynamic Devices for Suppressing Vortex-Induced Oscillation, J. Wind Eng. Ind. Aerodyn., 10 (1982) 21-29.